第 44 卷 第 4 期/2024 年 2 月/光学学报 封底文章·特邀综述

光学学报

多模态非线性光学显微成像技术研究综述

李艳萍，陈永强，刘雨晴，胡睿，屈军乐，刘丽炜*

深圳大学物理与光电工程学院，教育部/广东省光电子器件与系统重点实验室，广东 深圳 518060

摘要 介绍各种非线性光学显微成像的基本原理，并阐述非线性光学成像的多模态耦合所面临的技术挑战与解决方案。从成像速度、空间分辨率以及信噪比三个方面介绍了多模态非线性光学成像的研究进展，并扩展了多模态非线性光学内窥镜和图像分析方法。最后展望了多模态非线性光学成像的发展趋势和所面临的挑战，以期给相关领域研究人员提供参考。

关键词 成像系统；显微成像；非线性光学；多模态光学成像；光学内窥镜

中图分类号 TH742 **文献标志码** A **DOI**：10.3788/AOS231343

1 引 言

光学显微镜依据透镜成像原理实现了微小物体的放大成像，满足了人们观察微观世界、获取微观结构信息的需求。早在1590年，荷兰和意大利的眼镜制造商已经制造出类似显微镜的仪器，以实现物体放大。之后，随着偏光显微镜、干涉显微镜、相衬显微镜、共焦扫描显微镜和扫描隧道显微镜的发展，光学显微镜成为研究生物成像的重要工具，极大地促进了生命科学领域的发展。而非线性光学最早可追溯至1931年，Goppert Mayer首次在理论上对双光子吸收进行预测。1960年激光器问世，激光器可通过受激辐射形成高密度光子，即强相干光——激光。在高峰值功率脉冲激光作用下，光与物质在相互作用过程中出现了一系列不同于线性光学的新现象与新效应，主要包括二阶/三阶非线性混频、强光自聚焦、强相干光受激散射与多光子吸收等。非线性光学的快速发展也进一步推动了光学显微镜的发展，基于非线性效应的光学显微镜应运而生，其发展历程如图1所示。1974年，Hellwarth等[1]提出了二次谐波产生（SHG）显微镜并用于观察ZnSe晶体的空间结构变化。1982年，Duncan等[2]构建了相干反斯托克斯（CARS）显微镜，并实现了鼠耳组织中胶原纤维成像。1990年，美国康奈尔大学Webb小组[3]提出了双光子激发荧光（TPEF）显微镜，并对猪肾细胞中的DNA进行标记，观测活细胞中的染色体形态。1992年，Piston等[4]开发了一种双光子频域时间分辨扫描显微镜，即双光子荧光寿命显微镜（TP-FLIM），并在几秒的图像采集时间内记录了活细胞的荧光衰减时间图像。1996年，Xu等[5]提出了三光子激发荧光（3PEF）显微镜，选择960～1050 nm的激发波长实现了对Ca^{2+}指示剂、DAPI等探针的激发。2007年Ploetz等[6]发展了受激拉曼散射（SRS）显微镜，而2008年谢晓亮团队[7]实现了SRS显微成像的生物医学应用，观察了肺癌细胞以及鼠脑中的脂质、蛋白分布。非线性光学成像具有天然的衍射极限空间分辨率与光学切片效果，且多采用近红外激光光源激发，具有较强的组织穿透力和较小的光损伤体积，同时可提供组织的无标记成像，避免了外源性标记物引起的毒性。因此，近年来非线性光学显微镜（NLOM）[8]在生物医学领域得到广泛的应用。

在生物组织成像中，不同的生物分子具有不同的非线性光学特性，因此，不同的非线性光学成像模式具有分子特异性和分子选择性[9]。例如，多光子激发荧光（MPEF）显微镜可对一些内源性荧光团进行成像，如烟酰胺腺嘌呤二核苷酸（NADH）[10-11]、黄素腺嘌呤二核苷酸（FAD）[12]和弹性蛋白[13]等。SHG显微镜对具有非中心对称分子组织的生物结构高度敏感，已成功用于观察结构蛋白阵列，例如胶原蛋白[14]。三次谐波产生（THG）信号仅在介质中焦点体积标度内具有光学异质性时产生，可用于揭示脂质体[15]和组织内细胞核的存在。CARS和SRS显微镜提供分子振动状态的高分辨率图像，例如CH_n（n为氢原子数目）拉伸振动化学键（脂质和蛋白质中的主要化学键）。此外，多光子显微成像中的荧光寿命这一参量信息能够对微环

收稿日期：2023-08-01；**修回日期**：2023-09-19；**录用日期**：2023-09-26；**网络首发日期**：2023-10-23

基金项目：国家自然科学基金（62175163，62225505，61935012）、深圳市杰出青年基础科研项目（（RCJC20210706091949022）、深圳市重点项目（JCYJ20200109105404067）、中国博士后基金面上资助（2023M732347）

通信作者：*liulw@szu.edu.cn

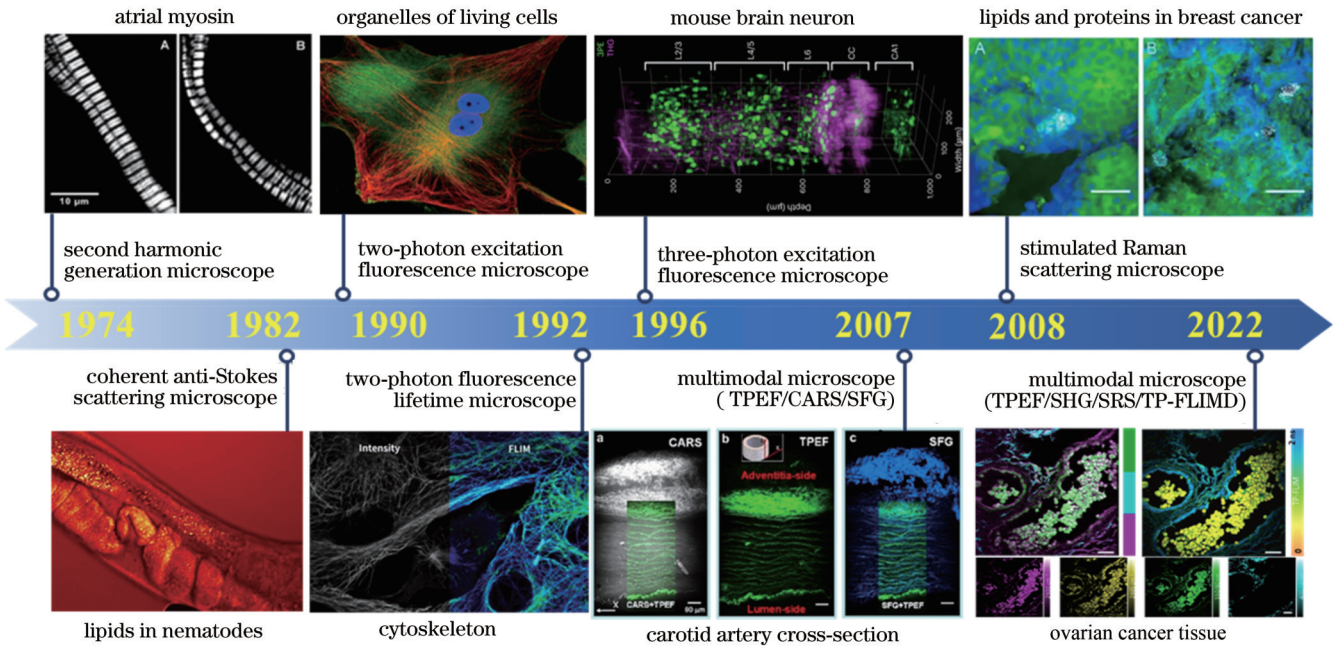

图 1　非线性光学显微镜发展历程

Fig. 1　Development history of nonlinear optical microscopes

境信息的改变进行定量分析，这些成像技术均可实现具有亚细胞空间分辨率的非接触式的实时生化信息获取。然而，随着人们对生命科学研究的不断深入，非线性光学成像技术的应用范围也逐渐扩大，而生物样本的结构与功能的复杂性需要从不同维度进行多参量信息的获取，以实现对其复杂生物过程的深入研究，因此，生物医学领域迫切需要能够获取多维度生化信息的光学成像技术，以实现对生物组织的多参量表征，获得更为全面的微观结构特性和功能信息。2007 年，程继新团队[16-17]将 TPEF、SHG 与 CARS 三种非线性光学成像方式整合在同一成像平台，实现了 TPEF、SHG 与 CARS 的多模态成像，用于研究健康和疾病状态下的中枢神经系统。之后，该团队在该系统上进一步扩充了 THG 成像，获得了 TPEF、SHG、THG 与 CARS 四模态非线性光学显微成像和拉曼光谱信息，实现了对动脉粥样硬化病变组织的病理信息分析[18]。2010 年，Sowa 团队[19]采用非线性多模态光学成像技术对动脉粥样硬化斑块的形成机制进行进一步分析，研究结果证明了巨噬细胞浸润与脂质积累加剧斑块的形成。随着激光光源、扫描器件以及探测器件等技术的发展，多模态非线性光学显微镜在成像速度、信息获取通量以及仪器小型化等方面得到了快速发展。其中，Anis 团队[20]采用微机电系统（MEMS）扫描镜和定制微型光学元件实现了新型小型化多模态光学成像平台。Qu 团队[21]通过光子晶体光纤获得超连续谱光源，并通过时间分辨和波长分辨检测技术实现了多元 CARS、TPEF 和 SHG 的同时成像。2015 年，该团队[22]将多光子显微成像与高光谱 SRS 成像系统进行集成，实现了转基因秀丽隐杆线虫的活体成像。2016 年，Boppart 团队通过扩展激发光源，实现了基于可编程超连续脉冲激发的集成 SHG、THG、TPEF 和 CARS 的多模态光学成像技术。2018 年，Dario 团队[23]采用光纤激光器作为光源，构建了包括 CARS、SRS 和 TPEF 的一种多模态非线性光学激光扫描显微镜，并将其应用于水生植物新鲜叶片的细胞壁和叶绿体的可视化。基于非线性效应的多模态光学成像系统快速发展，广泛应用于细胞检测[24-26]、药物传递[27-28]、癌症诊断[29-33]、脑成像[34-35]等生物医学领域[36]。

本文回顾了多种非线性光学成像的基本原理与对比机制，讨论了多模态非线性光学成像中多种模式耦合的技术发展，并从成像速度、空间分辨率以及成像信噪比等方面讨论了多模态光学成像的研究现状；进一步展示了多模态非线性光学内窥镜以及多参量图像分析方法；最后，对该技术未来的发展趋势进行讨论与展望。

2　典型非线性光学效应

非线性光学显微镜[8]是一种利用光和物质之间的非线性相互作用来对成像生物组织中的荧光和散射现象进行成像的技术。而多模态非线性光学显微成像技术是将多种非线性光学成像模式集成于一体，通过不同的对比机制获取生物样品中不同的内源性和外源性分子结构和功能信息。

非线性效应的激发需要来自超短脉冲激发光的聚焦，以获得非常高的峰值强度，多个光子同时到达激发荧光团或特异性结构时，二者将相互作用并产生非线

性光学信号。下面将对不同非线性成像模式的对比机制进行简要描述，主要包括多光子激发荧光、二次/三次谐波产生、相干拉曼散射等。图 2 为几种典型非线性光学效应产生过程的能级示意图，图中 h 为普朗克常量，υ_0 为激发光光子频率，υ_1 为信号光光子频率，f_1 为激发态低能级，f_2 为激发态高能级，g 为基态，i_1、i_2、i_3 为虚能级，ω_p 为泵浦光角频率，ω_s 为斯托克斯光角频率，ω_{as} 为反斯托克斯光角频率，Ω 为分子振动频率。

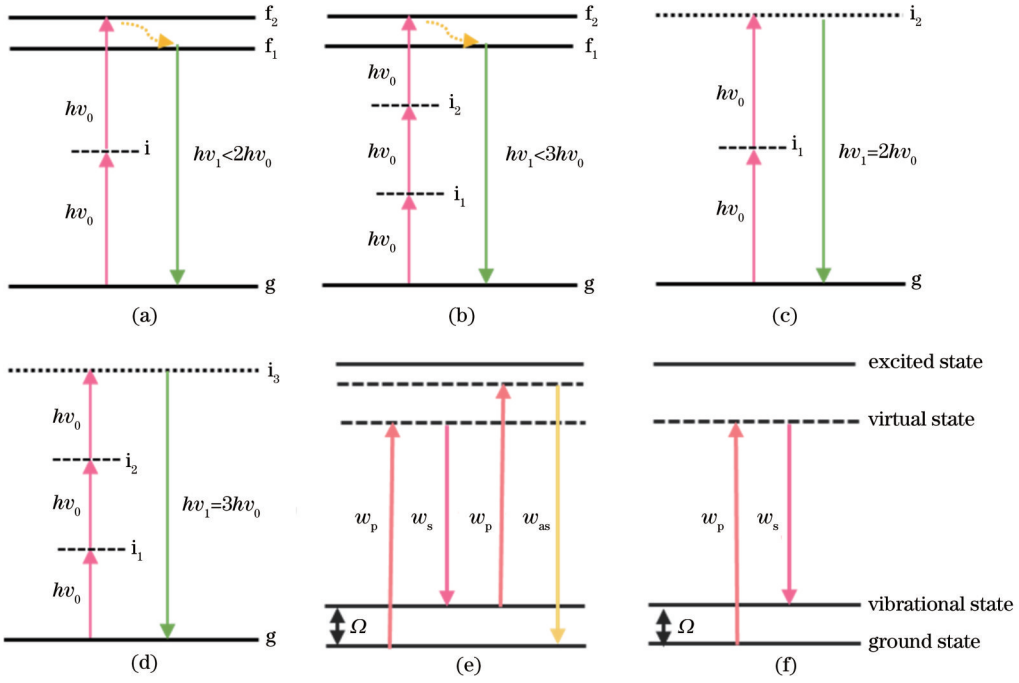

图 2　非线性效应产生过程的能级图。(a)双光子激发荧光；(b)三光子激发荧光；(c)二次谐波产生；(d)三次谐波产生；(e)相干反斯托克斯散射；(f)受激拉曼散射

Fig. 2　Energy level diagrams of nonlinear effect. (a) Two photon excitation fluorescence; (b) three photon excitation fluorescence; (c) second harmonic generation; (d) third harmonic generation; (e) coherent anti-Stokes scattering; (f) stimulated Raman scattering

不同于传统的单光子激发荧光显微镜，多光子激发荧光需要同时吸收两个或多个光子以激发荧光分子，利用该非线性过程进行显微成像的技术称为 MPEF 技术。类似于单光子激发荧光，在多光子激发荧光过程中，两个或多个光子被同一个分子吸收，其能量激发一个电子从基态 g 跃迁至激发态 f_2 后在短时间内弛豫到 f_1 态，在 f_1 态发射出一个新的光子并回到基态，如图 2(a)和图 2(b)所示。从非线性光学的半经典理论角度分析，在强相干光的入射作用下，在一种各向同性的非线性光学介质中，介质的电极化强度可表示为

$$P(\omega)=P^{(1)}(\omega)+P^{(3)}(\omega)+P^{(5)}(\omega)+\cdots=\varepsilon_0\left[\chi^{(1)}(\omega)E(\omega)+\chi^{(3)}(\omega,\omega,-\omega)E(\omega)E(\omega)E^*(\omega)+\chi^{(5)}(\omega,\omega,-\omega,\omega,-\omega)E(\omega)E(\omega)E^*(\omega)E(\omega)E^*(\omega)+\cdots\right],\tag{1}$$

式中：$E(\omega)$ 是角频率为 ω 的入射单频光波电场矢量强度；$E^*(\omega)$ 是 $E(\omega)$ 的复共轭函数；$\chi^{(1)}$ 为介质的线性电极化率，其实部表征介质的普通折射率，虚部表征普通单光子吸收；$\chi^{(3)}(\omega,\omega,-\omega)$ 代表该介质的三阶非线性电极化率，实部表征与入射光强成正比的感应折射率变化，虚部表征双光子吸收过程；$\chi^{(5)}(\omega,\omega,-\omega,\omega,-\omega)$ 表示五阶非线性电极化率，其实部描述了与入射光强平方成正比的折射率变化，虚部描述了三光子吸收过程。依据上述理论，双光子吸收属于三阶非线性过程，三光子吸收属于五阶非线性过程。

在 MPEF 中，多光子激发的荧光分子遵循与单光子激发相同的衰减过程，从而发出相同的特征荧光信号。而荧光寿命是指大量荧光分子从激发态衰减至基态的平均时间，常用 τ 表示。荧光寿命取决于荧光分子的构象与其所处环境，是荧光物质的固有性质，可用作荧光团所处微环境中各种生物物理和化学参数的定量传感器，如 pH、黏度、温度、离子浓度和化学反应动力学[37-38]。TP-FLIM 作为 TPEF 成像的扩展，通过寿命测量与显微成像的结合可从另一个信息维度对生物样品进行表征与分析，使其成为一种强大的定量成像技术。TP-FLIM 的一个关键优势是其图像对比度源于荧光寿命的测量值，这在很大程度上独立于荧光信号强度和荧光团浓度，被广泛应用于高通量、高内涵药物的筛选、临床诊断，以及生化反应研究。

二次谐波产生[39]、三次谐波产生[40]过程为二阶/三阶非线性混频效应。其中，SHG是一种二阶非线性混频过程，两个入射光子与材料相互作用并转换为一个发射光子，具有两倍的激发光子能量，即双倍频。而THG是一种三阶非线性混频过程，是指三倍光频。不同于TPEF和3PEF，SHG和THG过程中并没有光子的吸收，该过程中非线性介质扮演着能量转换器的作用，是一个参量过程，如图2(c)和图2(d)所示。SHG发生在非中心对称结构中，而生物体中一些组织(如胶原[41]、微管[42]和肌球蛋白[43])表现为该结构，因此，SHG已经被用于特异性组织结构成像。THG发生在折射率或三阶磁化率在焦点处有显著变化的组织结构中，例如：在生物组织中，在水/脂质界面折光指数具有显著变化，因而能够实现脂质[44]、髓鞘[45]、细胞膜[46]、骨骼[47]和其他组织界面的无标记THG成像。

CARS和SRS显微成像原理均基于相干拉曼散射(CRS)，可从分子振动模式中获得其成像对比度，被广泛用于生物分子识别与分析。相比于自发拉曼散射，CRS利用相干非线性激发提高拉曼过程的量子效率，有效增强了拉曼散射信号，可大幅度缩短成像时间，其过程如图2(e)和图2(f)所示。其中，泵浦光(频率为ω_p)和斯托克斯光(频率为ω_s)与物质发生作用，产生频率为ω_{as}的CARS信号，此过程为参量过程，当泵浦光与斯托克斯光的频率差和分子振动频率Ω相匹配时，CARS信号将得到增强，该过程为三阶非线性混频。然而CARS过程会伴随着非共振的四波混频信号，该非共振背景导致CARS光谱与自发拉曼光谱相比有一定畸变，因而很难实现指纹区成像。SRS是一个能量转移过程，该过程中泵浦光湮灭一个光子而斯托克斯光产生一个光子，这两种现象分别称作受激拉曼损耗(SRL)和受激拉曼增益(SRG)，为强光受激散射效应。由于不受非共振背景的影响，在SRS成像中所获得的拉曼光谱的线型与自发拉曼散射较为一致。大多数相干拉曼散射技术研究的是高波数CH化学键(波数范围为2800～3100 cm^{-1})，该区域包含大量高强度、光谱较宽的拉曼峰，对应于CH_n振动。与CH区相比，低波数指纹区(波数范围为600～1800 cm^{-1})包含丰富的分子键，如O—H、C—C、C=C和C=O，谱线宽度通常小于10 cm^{-1}，该区域拉曼峰的密集分布和较低的信号强度对CRS系统的光谱分辨率和激发强度提出了更高要求。近年来，人们开始关注位于指纹区和高波数区域之间的静默区域，这推动了具有高特异性和高灵敏度的拉曼探针技术的发展。例如同位素标记[48-49]、三键振动标记(C—D，C≡C，C≡N)[50-51]、拉曼活性纳米材料和多重拉曼染料[52]等。随着成像系统和拉曼探针的发展，CRS显微成像技术被广泛应用于细胞、肿瘤、神经科学以及微生物学等生物医学领域的各个分支。

表1汇总了上述非线性光学显微成像技术的特征，并进行对比分析[1-5,7,53]。不同的非线性光学显微技术能够成像特定的分子或结构，将多种非线性成像技术(MPEF、SHG、CRS等)耦合，可从组织结构、分子代谢等多维度对生物体进行成像分析，因此，多模态非线性光学成像的发展将为复杂生物体的研究提供了一个重要手段。

3 非线性光学显微成像技术的多模式耦合

3.1 MPEF、SHG和THG三种成像模式耦合

非线性光学复合成像技术能够获取生物体的多种非线性光学特征，是从多维信息角度研究复杂生物体与多线程动态过程的重要工具。而多种非线性光学成像技术集成的关键在于多种非线性效应的同步激发与多维信号同时探测的协调。对于MPEF和多次谐波成像，通常选择近红外超短脉冲(飞秒光源)激发并采用二向色镜与滤光片组合以波长分离的方式实现多种成像模式的耦合，如图3所示。van Huizen团队[54]采用对应波长参数的光学滤光片以波长分离的方式实现了THG、SHG和双光子自荧光(2PEF)的同时成像，该方法可用于分析新的人体肺部肿瘤的组织病理学信息。基于MPEF、SHG和THG的多模态非线性光学显微镜可探测生物组织的内源性物质的光学特性，被应用于活斑马鱼胚胎细胞分裂、活体秀丽隐杆线虫等无标记微观生物研究[55]。此外，THG/SHG成像可提供人眼角膜中间质微结构信息，而THG/2PEF信号反映了角膜细胞网络的状态，因此，该多模态成像技术能够揭示与生理相关的人眼角膜的非线性光学特性，提供青光眼生理病理的重要信息[56]。另一方面，SHG成像主要来源于胶原蛋白，3PEF和THG信号来自多种组织结构与细胞内成分，包括脂肪结缔组织和红细胞的强信号，而2PEF成像可揭示代谢辅酶NADH与FAD，该多模态非线性光学显微镜可进行卵巢癌[57]、乳腺癌[58]等病理组织分析，为癌症的早期诊断提供重要病理信息。多光子、二次/三次谐波多模态光学显微镜可以作为生物成像分析的重要手段，波长可调谐和可有效激发非线性效应的超快激光器对于非线性光学成像至关重要。中国科学院物理研究所北京凝聚态物理国家实验室采用光纤的自相位调制特性，将掺镱/铒光纤激光器(YDFLs/EDFLs)的窄带输入光谱拓宽，获得了1300～1700 nm的快速波长可调飞秒光源，并实现了人体皮肤组织与脑组织的多参量光学成像[59]。

3.2 FLIM、MPEF和SHG三种成像模式耦合

FLIM成像可在多光子成像的基础上通过增加寿命探测模块实现，主要包括时间相关单光子计数(TCSPC)[60-61]以及频域法FLIM[62-63]。为了实现高时间分辨的荧光寿命测量，通常采用基于TCSPC的荧光寿命成像。在该过程中，荧光分子被光脉冲激发到激发态，再从激发态衰减到基态，以激发光脉冲为参

表 1 非线性光学显微镜的特征

Table 1 Characteristics of nonlinear optical microscopes

Imaging modality	TPEF	3PEF	SHG	THG	CARS	SRS	FLIM
Electric susceptibility	χ^3	χ^5	χ^2	χ^3	χ^3	χ^3	—
Year of discovery	1961	1967	1961	1962	1965	1962	1989
First application	1990[3]	1996[5]	1974[1]	1997[53]	1982[2]	2008[7]	1992[4]
Contrast mechanism	Two-photon simultaneous absorption	Three-photon simultaneous absorption	Non-centrosymmetric structure	Structures with significant changes in refractive index or third-order magnetic susceptibility	Molecular vibration		Conformation of fluorescent molecules and their environment
Typical applications	NADH, FAD, etc.		Structural protein array, collagen fibers, etc.	Liposomes, adipose tissue, etc.	Biomolecules such as lipids and proteins		PH, viscosity, temperature, ion concentration, etc.
Features	High resolution, 3D tomography capability, large imaging depth, qualitative analysis of specific molecules		High sensitivity, high signal-to-noise ratio, and no involvement in light absorption, without thermal damage and photobleaching		High sensitivity, high specificity, spectral resolution, but complex imaging system		Not affected by fluorescence concentration, photobleaching, and excitation light intensity, with quantitative analysis ability

考,对光子到达探测器的时间进行统计。光子在大量脉冲上迭代计时,直到每个像素上能够收集到足够的光子数(通常超过 100 photon/pixel)。对于每个像素,光子到达时间被分类成一个直方图,该直方图表示荧光衰减的概率密度函数,从而实现荧光寿命信息测量。作为 MPEF 的信息维度扩展,FLIM 成像能够完美地与其他非线性光学成像实现多模式耦合[64-66]。深圳大学刘丽炜团队开发了基于可调谐激光器和多通道探测器的多维非线性表征以及荧光寿命的多模态成像平台,通过 3PEF 和 2PEF 分别获得 NADH 和 FAD 成像分布以分析癌症转移区域,通过胶原纤维的 SHG 信号来分析肿瘤的侵袭过程,通过基于单光子激发的 phasor-FLIM 来揭示胰腺癌组织的代谢变化,证明了该系统可用于研究转移性肿瘤的病理机制和生化过程分析,如图 4 所示[64]。该团队在上述系统的基础上进一步扩展了 TP-FLIM 成像模块,结合 MPEF 与 SHG 成像对临床卵巢癌病理组织的转移路径[67]、代谢特征[66]进行分析,获得早期卵巢癌的生理信息,实现了浆液性卵巢癌病理分期,为辅助临床诊断提供有用数据。MPEF 与 SHG 成像能够揭示组织结构特征,获得生物体微观形态特征,而 FLIM 成像技术是微环境信息监测的重要工具,因此,集成 MPEF、SHG 与 TP-FLIM 的多模态成像被广泛应用于各种疾病病理组织的诊断分析,例如结肠癌[68]、动脉粥样硬化[68]、乳腺癌[69]等。

3.3 CARS/SRS、MPEF 和 SHG/THG 多种成像模式耦合

CARS 显微镜的实现需要两束激发光(泵浦光与斯托克斯光)在空间与时间共线的光学配置,且 CARS 成像技术的信号强度与特异性相互制约[70],即超短脉冲具有更高的峰值功率,能产生较强的 CARS 信号,同时也将产生较强的非共振背景,而较长脉冲激发将造成信号强度较低,但具有高的光谱分辨率与特异性[70-71]。为了实现 CARS 与多光子荧光显微镜的耦合,Chen 团队[72]和 Pegoraro 等[73]采用飞秒脉冲作为激发光源实现了 MPEF、谐波与 CARS 的多模态非线性光学成像,验证了该系统能够同时可视化复杂生物系统中的不同结构[74]。Langbein 等[75]在宽带飞秒脉冲激发系统中采用光谱聚焦[76]方案满足了 CARS 成像的高

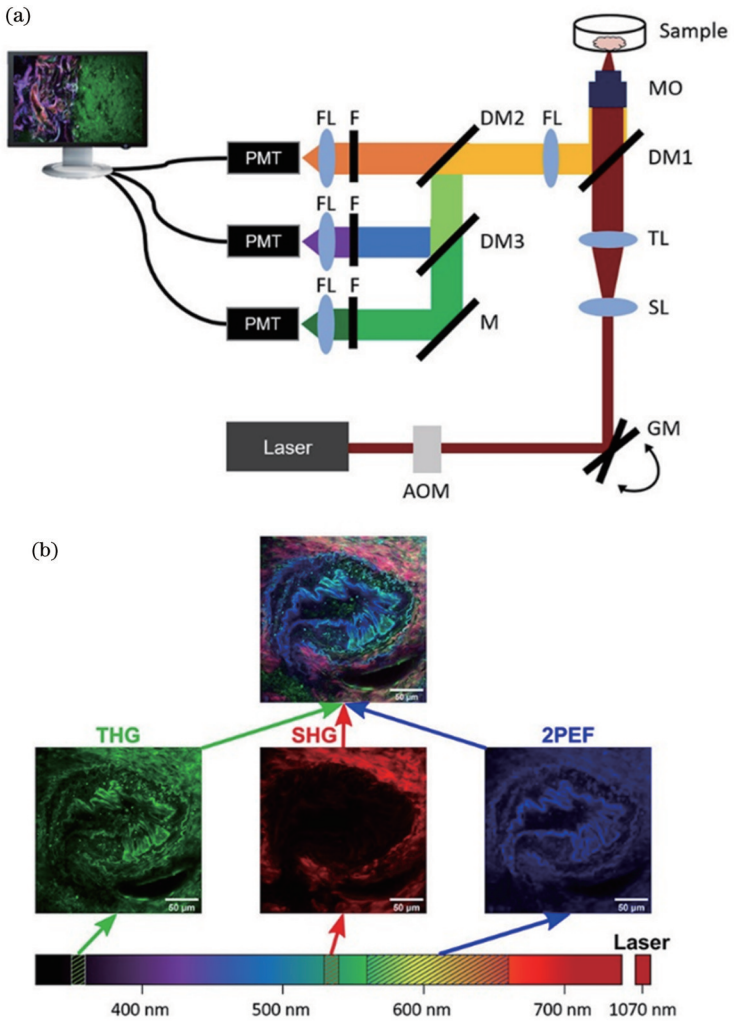

图 3　多光子与二次谐波显微成像[54]。(a)光学系统原理图(AOM:声光调制器;GM:振镜;SL 和 TL:扫描和管透镜;DM:二色镜;M:反射镜;MO:显微镜物镜;FL:聚焦透镜;F:滤光片;PMT:光电倍增管);(b)肺肿瘤组织的 THG、SHG、2PEF 信号通过适当的滤波器实现波长分离,并合并成一张 THG/SHG/2PEF 图像

Fig. 3　Multiphoton and second harmonic optical microscopy[54]. (a) Schematic diagram of optical system (AOM: acousto-optic modulator; GM: galvanometer; SL and TL: scan lens and tube lens; DM: dichroscope; M: reflector; MO: microscope objective; FL: focusing lens; F: filter; PMT: photomultiplier tube); (b) THG, SHG, and 2PEF signals of lung tumor tissue are detected by wavelength separation method with appropriate filters and merged into a THG/SHG/2PEF multi-modal image

光谱分辨率与高信号对比度。此外,在激发光路中采用双路 4*f*光栅对实现激发光束在皮秒与飞秒脉冲之间的切换,以分别实现高光谱分辨的 CARS 成像和高对比度的多光子成像[77]。多种非线性信号的同时采集是多模态成像的关键问题,可利用非线性信号的相干性来解决。CARS 信号大部分是前向散射,具有很强的方向性,因此,前向 CARS(F-CARS)信号可以通过高数值孔径(*NA*)进行高效采集[78-79]。而荧光信号频谱较宽且非相干,具有高数值孔径的聚焦物镜可以有效地收集反向荧光,因此可以使用两个光电倍增管(PMT)同时记录 F-CARS 信号和后向多光子信号,如图 5(a)所示。此外,多光子激发荧光、多次谐波以及 CARS 信号也可通过增加 PMT 和选择合适的带通滤波器进行后向探测[80-83],如图 5(b)所示。CARS 成像能够获取生物体内脂质、蛋白质等生物大分子的分布与含量信息,因此,集成 CARS、SHG、THG 与 MPEF 的多模态成像系统被广泛应用于与脂质变化相关的疾病成像分析,包括与脂质沉积相关的动脉粥样硬化[19, 84-85],通过分析 CH 拉伸区域内的 CARS 光谱,就可以证明动脉组织标本中弹性纤维、甘油三酯、胶原、髓磷脂、细胞质和脂滴的分化[86-87]。Boppart 团队[88-89]使用一种新型光子晶体光纤源来产生可编程超连续脉冲,搭建了集成 CARS、MPEF 和 SHG/THG 的无标记多模态光学显微成像平台,获得新鲜的离体乳腺组织的光学特征以研究介观生物组织、肿瘤细胞迁移和(淋巴)血管生成,验证了该平台在无染色组织病理分析的临床应用潜力。此外,该类型多模态成像系统可分析组织中聚集的肝脂肪、胶原纤维和细胞形态,为肝

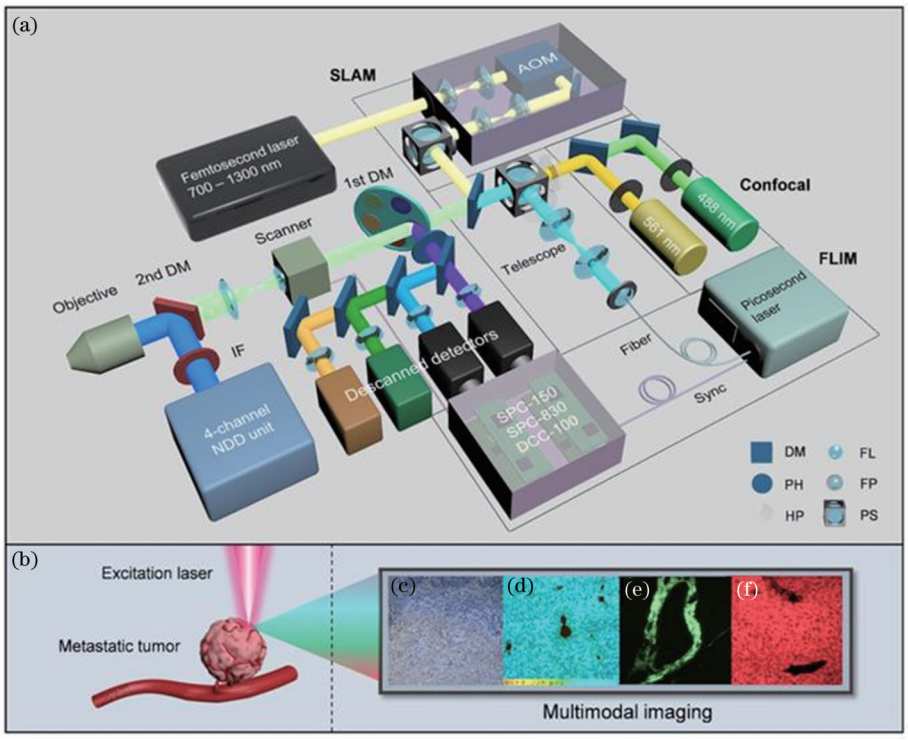

图 4　多模态光学显微成像系统用于分析原发性和转移性肿瘤微环境[64]。(a)基于 MPEF/SHG/THG 和单光子 FLIM 的光学成像系统原理图(AOM:声光调制器;IF:近红外截止滤光片;DM:二向色镜;PH:针孔;HP:半波片;FL:聚焦透镜;FP:光纤端口;PS:偏振分束器);(b)转移性肿瘤的无标记成像;(c)NADH 的 3PEF 图像;(d)FLIM 图像;(e)胶原蛋白的 SHG 图像;(f)FAD 的 TPEF 图像

Fig. 4　Multimodal optical imaging microscopy is used to analyze the primary and metastatic tumor microenvironment[64]. (a) Schematic diagram of the optical imaging system based on MPEF/SHG/THG and single photon FLIM (AOM: acousto-optic modulator; IF: IR-cut filter; DM: dichroic mirror; PH: pin hole; HP: half-wave plate; FL: focal lens; FP: fiber port; PS: polarization splitter); (b) label-free imaging of metastatic tumors; (c) 3PEF image of NADH; (d) FLIM image; (e) SHG image of collagen; (f) TPEF image of FAD

脏脂肪变性和纤维化[90]、喉癌[91]、皮肤癌[92]等疾病的早期诊断和检测提供有效的手段。

SRS 和 CARS 的激发条件相同,在成像过程中同时发生,但 SRS 信号来自斯托克斯光束的强度增益(SRG)或泵浦光的强度损耗(SRL)。由于 SRS 过程所引起的被检测光束强度的微小变化被埋没在噪声中,因此需要通过锁相放大器进行相敏检测以恢复信号。以 SRL 信号的高速检测为例,斯托克斯光束通常在 MHz 频率下进行强度高频调制以避免低频激光噪声[7, 93],泵浦光由大面积光电二极管检测。在该过程中,被检测光束的噪声限制了系统的极限灵敏度。不同 CARS 信号出现一个新的波长,可采用二向色镜与滤光片隔离其他信号,SRS 信号与激发光束具有相同的波长,因此,SRS 成像通常为透射式的前向信号探测,也可采用偏振分离的方式实现后向 SRS 信号检测[94]。依据激发条件与探测方式,SRS 成像被证明可以实现与 MPEF、SHG 以及 CARS 等多种成像的耦合,在成像系统中,MPEF、SHG 和 CARS 可采用 PMT 实现后向检测,SRS 可采用光电二极管实现前向探测[95-98]。

3.4　CARS/SRS、MPEF、SHG/THG 和 FLIM 多种成像模式耦合

在多模态非线性光学成像系统中,各模式成像所需激发条件不同,通常需要采用不同的激发条件进行顺序成像[82, 99-100]。例如,Weber 团队[99]提出一种无标记的多模态非线性成像方法,能够同时获得 TPEF、CARS、SHG 图像,之后利用基于 TCSPC 的 FLIM 对 CARS 图像的自体荧光背景进行校正。多维信息顺序采样方式耗时长,易造成样品的光漂白与光损伤;此外,成像效果也容易受到激光器的功率波动以及环境扰动的影响。因此,实现多参量非线性光学成像信息的同时获取需要克服以下挑战:1)高激发效率的多光子荧光、谐波与高光谱相干拉曼成像需要不同的激发条件。皮秒激发光源会不可避免地导致 TPEF 和 SHG 成像的光子产率偏低,特别是对于 3 阶非线性效应的 THG 和 5 阶非线性效应的 3PEF,其激发效率更低,尤其是在基于 TCSPC 的 TP-FLIM 成像中,皮秒激发将需要更长的光子累积时间来获得足够的光子数。2)多种非线性过程同时存在时,其信号之间存在一定的串扰。例如:若采用飞秒脉冲激发 TPEF 和

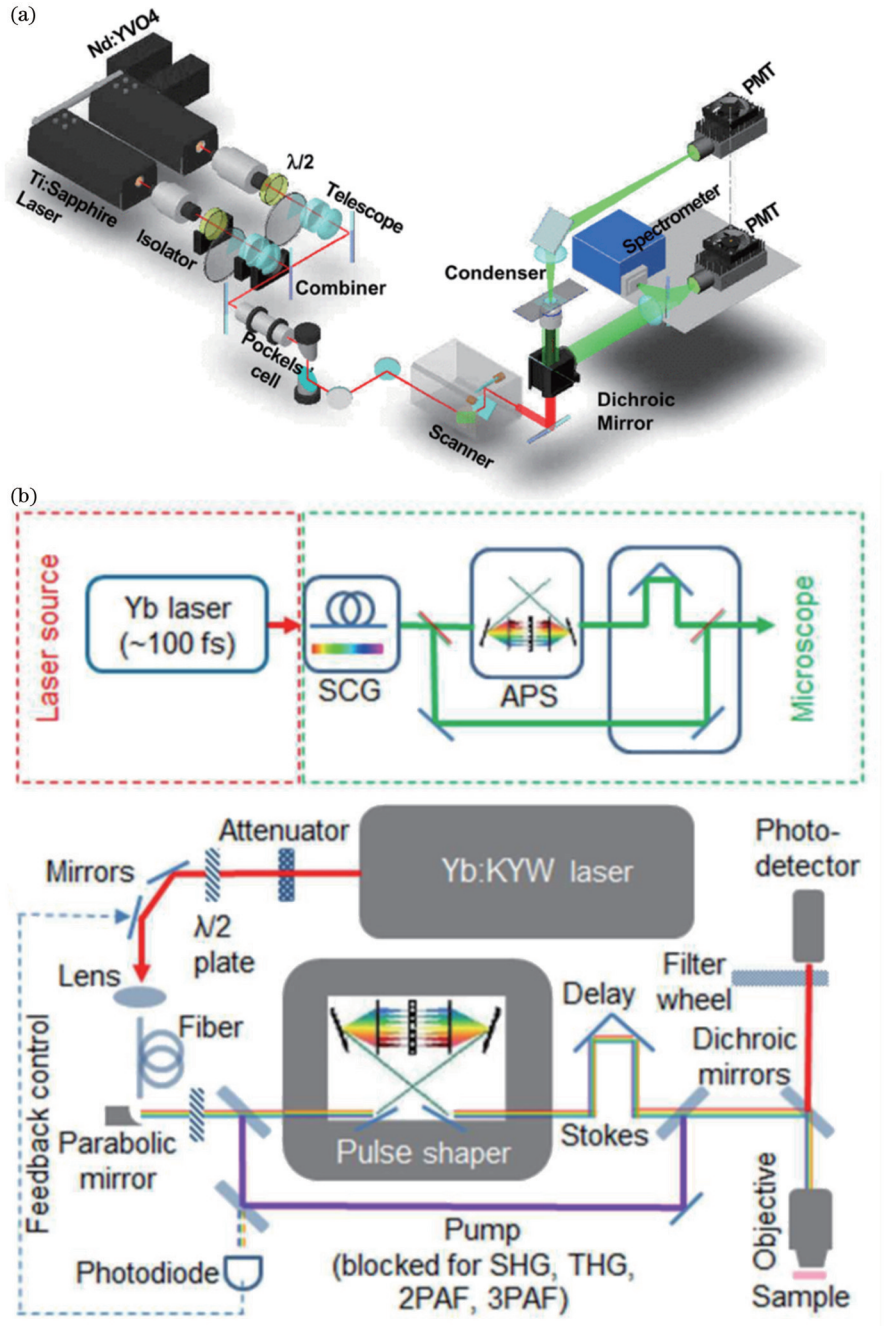

图 5　非线性光学成像系统中的 MPEF、SHG/THG、CARS 多模式耦合。(a)集成 TPEF、SHG 以及 CARS 的多模态非线性光学成像系统(PMT:光电倍增管)[81];(b)集成 TPEF、3PEF、SHG、THG 以及 CARS 的多模态非线性光学成像系统(SCG:超连续谱产生;APS:任意脉冲整形)[82]

Fig. 5　Multi-mode coupling of MPEF, SHG/THG, and CARS in nonlinear optical imaging systems. (a) Multimodal nonlinear optical imaging system that integrates TPEF, SHG, and CARS (PMT: photomultiplier)[81]; (b) multimodal nonlinear optical imaging system that integrates TPEF, 3PEF, SHG, THG, and CARS (SCG: supercontinuum generation; APS: arbitrary pulse shaping)[82]

SHG(高效率)并采用皮秒脉冲激发 SRS(高光谱),则飞秒脉冲将增加皮秒探测光(泵浦光)的基底信号,使得 SRS 探测光解调效率降低,导致了 SRS 成像的信噪比与对比度的降低。此外,为了减弱热效应和光漂白,需要在时间上排列飞秒脉冲和皮秒脉冲,这将导致在 TP-FLIM 成像过程中,荧光寿命成像出现两个仪器响应函数,寿命曲线出现明显卷积,难以获得准确的寿命值。针对上述问题,深圳大学刘丽炜团队[101]在其前期工作基础上,提出偏振分离、皮秒分光、飞秒与皮秒超短脉冲的多路复用等方法,有望突破这些非线性多模态和荧光寿命的技术瓶颈,完成多参量非线性光学高分辨成像,如图 6 所示。这种同步成像机制加快了术中病理组织实时评估的过程,避免了多次激发引起的光漂白和光损伤,以其优越的空

间、光谱和时间分辨率，实现内源性物质、脂质蛋白葡萄糖等分子代谢以及癌细胞的氧化还原代谢变化等多参量信息的实时获取，用于全面评价肿瘤的病理特征[101-102]。

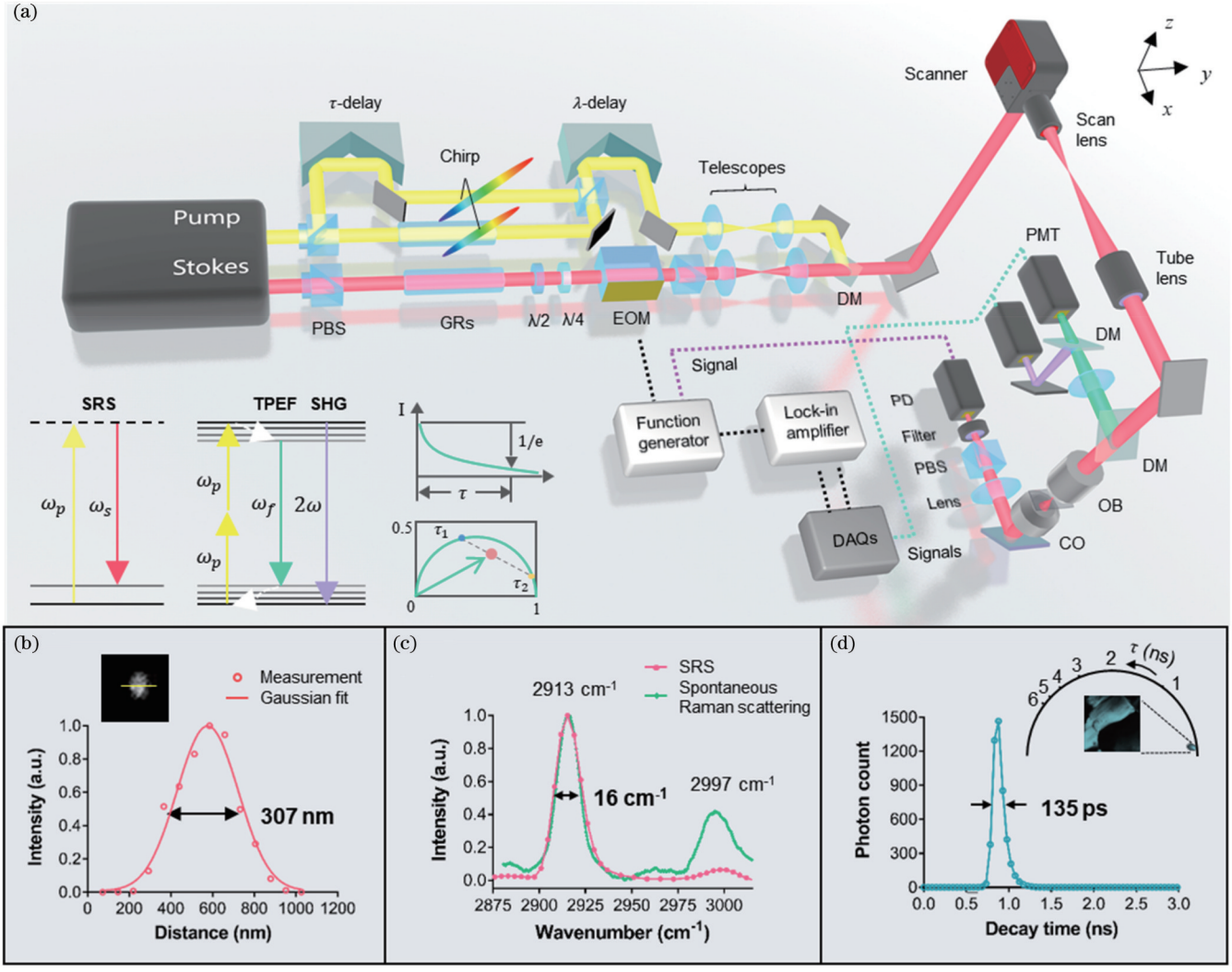

图 6　集成 TPEF、SHG、SRS 和 TP-FLIM 的多参量光学成像系统[102]。(a)系统原理图(CO：聚光镜；DAQ：数据采集卡；DM：二向色镜；EOM：电光调制器；GR：玻璃棒；λ/2：半波片；OB：物镜；PBS：偏振分束器；PD：光电二极管；λ/4：1/4 波片)；系统的(b)空间分辨率，(c)光谱分辨率与(d)时间分辨率

Fig. 6　Multi-parameter optical imaging system that integrates TPEF, SHG, SRS, and TP-FLIM[102]. (a) System schematic diagram (CO: condenser; DAQ: data acquisition system; DM: dichroic mirror; EOM: electro-optic modulator; GR: glass rod; λ/2: half-wave plate; OB: objective; PBS: polarizing beam splitter; PD: photodiode; λ/4: quarter-wave plate); (b) spatial resolution, (c) spectral resolution, and (d) temporal resolution of system

4　多模态非线性光学显微成像系统的优化

4.1　成像速度提升

基于不同非线性光学对比机制的高分辨多参量光学显微成像方法在生物医学中已经得到广泛的应用，但提高成像速度以实现高通量光学成像是技术创新的重要方向，数据吞吐量的提高对快速动力学过程研究[103-105]、快速临床诊断研究[106-108]，以及生物体复杂功能信息研究[101, 109]等都具有重要意义[110]。非线性光学显微镜通常采用点激发扫描来获取样品信息，因此，扫描器的更新速率是决定成像速度的重要因素。然而，对于多光子吸收这一类非线性过程，其成像速度也受到激发态寿命的限制，激发态寿命决定了每个分子产生光子信号的最高速率，该速率进一步决定了在每个像素上获得足够的信噪比所需的像素驻留时间。另一方面，光子产生速率随激发光功率的变化而改变，而光子能量被激发过程中的化学反应所产生的活性氧是引起分子光漂白和样品光损伤的重要因素[111]，这就限制了成像系统可使用的最高激发功率和像素驻留时间。综合上述分析，在不需要考虑延长像素驻留时间以确保图像信噪比时，可通过提高扫描器的速度和并行探

测成像这两种方式来提高非线性光学显微镜的吞吐量。

当每个像素上信号光子产生速率足够高，不需要考虑延长像素驻留时间以确保图像信噪比时，快速扫描器是提高显微镜成像速度最直接的方法。高通量非线性光学显微镜采用快速的机械扫描装置替代速度较慢的检流振镜扫描，如多边形扫描器和共振扫描器。图 7 为基于高速扫描器的高通量非线性光学成像系统[112-114]。具体地，多边形扫描器由一个精密加工的圆柱体组成，圆柱体周边有反射镜面，其旋转由高速电机通过空气轴承驱动。典型的多边形扫描仪有几十个镜像面，达到每分钟数万转的旋转速度。因此，多边形扫描器能够以每秒数万条扫描线的速度生成图像，提供超视频速率的成像[112, 115]。基于多边形扫描器的非线性光学显微镜的结构如图 7(a)所示，多边形扫描器用于一个轴扫描(X扫描)，采用扫描速度较小的检流镜沿正交方向扫描(Y扫描)。入射到多边形扫描器上的飞秒激光被扫描器偏转，并通过 $4f$ 系统入射到 Y 方向的检流扫描镜。沿一个方向的角输出由多边形的旋转角度决定，而另一个方向则由检流计的扫描角度决定。共振扫描器可以实现反射镜在确定的频率下振荡，角度位置为正弦变换，频率由其机械设计决定。基于共振扫描器的非线性光学显微系统的结构设计与多边形扫描器类似[116]，但这两类扫描器均缺乏位置和速度的精准控制，不能在给定的时间对特定的角度定位，因此需要由独立的传感器进行实时位置反馈。此外，声光偏转器(AOD)也可作为非线性光学显微镜的扫描装置[113]，如图 7(b)所示。相比于机械扫描器，基于 AOD

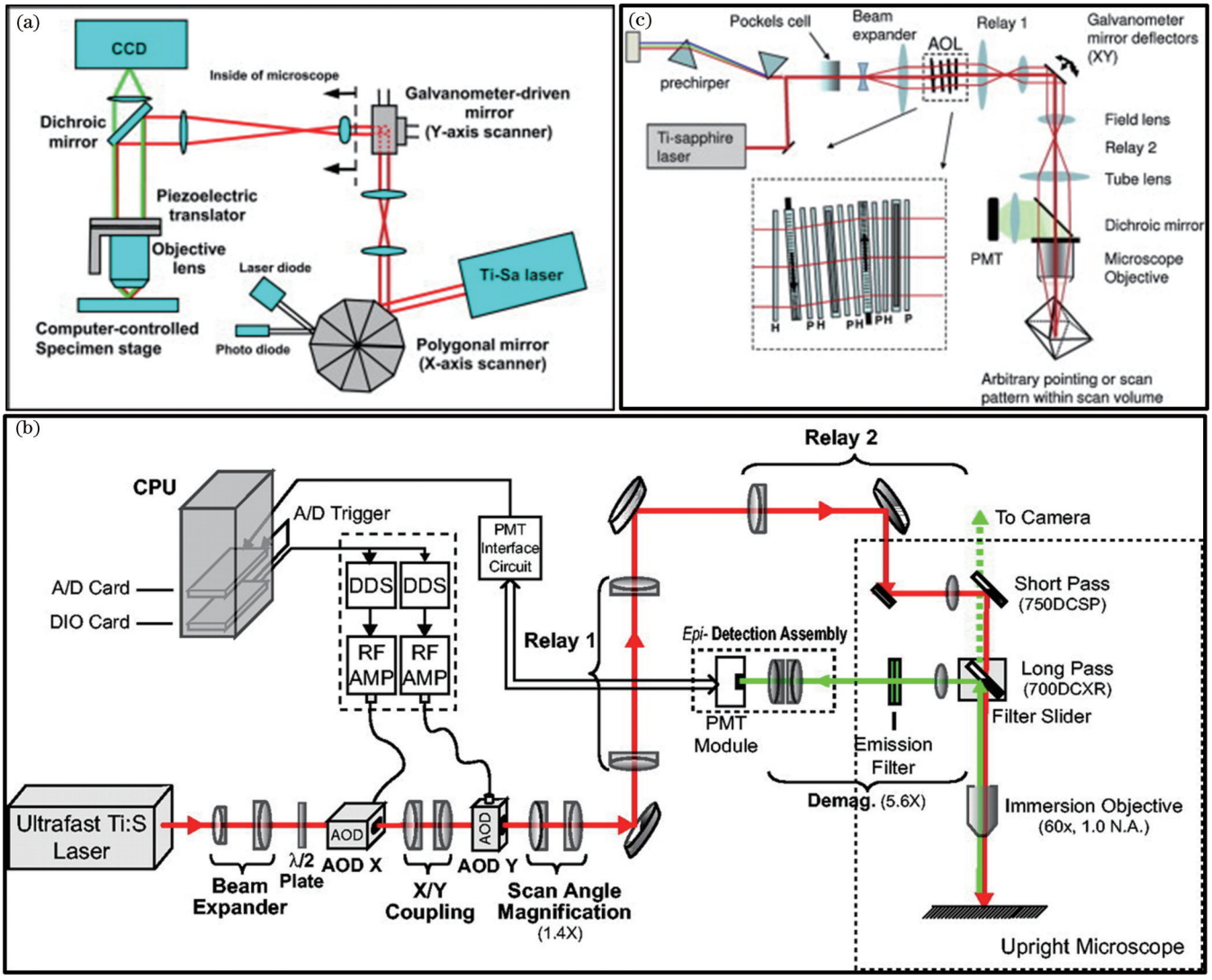

图 7　基于高速扫描器的高通量非线性光学成像系统。(a)基于多边形扫描器的非线性光学显微成像系统原理图[112]；(b)基于声光偏转器的非线性光学显微成像系统原理图[113]；(c)基于声光偏转器与检流镜的三维非线性光学体成像系统原理图[114]

Fig. 7　High throughput nonlinear optical imaging system based on high-speed scanner. (a) Schematic diagram of a nonlinear optical microscopy imaging system based on a polygonal scanner[112]; (b) schematic diagram of a nonlinear optical microscopy imaging system based on an acoustooptic deflector[113]; (c) schematic diagram of a three-dimensional nonlinear optical volume imaging system based on an acoustooptic deflector and a flow detection mirror[114]

的非线性光学显微镜能够随机访问二维平面内的不同位置，因此该扫描方式适用于对样品中感兴趣区域的快速动态过程的监测[104]，并且该方法可进一步扩展至三维体积的随机访问扫描，如图 7(c)所示。

多焦点激发[117-118]与宽场成像等并行探测是提高成像速度的另一种重要模式。多焦点激发系统中可使用透镜阵列、分束器系统[119]、声光偏转器或衍射光学元件[120]并行产生焦点数组。但不同焦点之间功率不均匀、衍射光学元件易受色散与色差的影响以及相邻焦点之间的光干扰等问题对图像对比度、信噪比以及分辨率均有影响。此外，宽场成像结合时空聚焦[121]、串行时间编码[122]以及全内反射激发[123]方法在不同程度上提高了成像速度，并保证了可观的图像对比度、信噪比和分辨率。

4.2 空间分辨率提升

非线性光学显微成像通常采用近红外光源激发，较长的波长激发增大了穿透深度并使光损伤最小化，但同时也降低了空间分辨率。然而，研究人员已经在线性光学显微镜中引入了多种超分辨率成像方法，例如受激发射耗尽(STED)、结构光照明显微成像(SIM)[124]，以及随机光学重构显微技术(STORM)，其分辨率可提高至 20～50 nm[125-127]。非线性光学显微成像的超高分辨率方案的研究重点是将超分辨模式与非线性激发机制结合。近年来，亚衍射极限成像方法被应用于 TPEF 显微镜，提高了超出衍射极限的分辨率。其中，STED 与非线性激发的结合需要具有斯托克斯红移的发色团，基于 STED 技术的超分辨 TPEF 显微镜的空间分辨率比普通双光子显微镜提高了 4～6 倍，并且可以在活细胞中同时进行双色超分辨成像[128]。此外，结构光照明与时间聚焦相结合能够提高深层组织双光子荧光成像的分辨率，与传统的时间聚焦显微镜相比，横向分辨率和光学切片能力分别提高了 1.6 和 1.4 倍[129]。相干拉曼散射显微成像需要两束近红外激光进行激发，可提供衍射极限分辨率，CARS 或 SRS 的横向分辨率为 300～400 nm。实验中，可通过采用可见光范围内的激发光束以及高数值孔径(NA=1.49)的油浸物镜来达到 200 nm 的空间分辨率[130-131]，但该方法舍弃了近红外激发所具备的穿透深度的优势。此外，超分辨 CRS 显微成像可以借鉴受激发射损耗(STED)成像原理，例如，通过引入第三束甜甜圈状的光束抑制 SRS 信号[132-135]，其理论成像分辨率可达到 50 nm[136]。另一方面，具有高化学分辨率的光开关受激拉曼散射探针能够实现在光活性拉曼频率下产生“开”或“关”的 SRS 图像，也有望实现超分辨率 SRS 成像[137-139]。近年来，深度学习的飞速发展也为超分辨 CRS 显微成像提供了思路。2023 年，Bintu 团队[140]将基于自适应矩估计(Adam)优化的点化反卷积(A-PoD)算法应用于 SRS 显微成像中，并证明了在单个脂滴(LD)膜上的空间分辨率低于 59 nm。

4.3 成像信噪比提升

对于基于非线性效应的多模态光学成像系统，限制其成像速度的关键在于复杂的机械和光学扫描装置。尽管可通过配置高速精密的机械扫描仪实现快速成像，但是所得到的图像信噪比低、分辨率不足和存在扫描伪影。针对这一问题，深圳大学刘丽炜团队提出了基于自对准注意引导残差中的残差密集生成对抗网络的深度学习自荧光谐波显微技术，同时兼顾成像速度、视场、空间分辨率以及图像信噪比。利用该神经网络框架将低 NA 物镜聚焦和高速共振扫描所获得的低分辨率、低信噪比的临床卵巢癌多模态图像进行图像增强，所得结果验证了该方法具有提升空间分辨率和缩短成像时间的优势。其中，注意引导的残余密集连接最大限度地减少了持续的噪声、失真和扫描条纹，从而降低了荧光与谐波图像的质量，并避免了输出图像中的重建伪影。该方法具有高对比度、高保真度、图像重建速度快等优点，结合非线性多模态成像平台可作为无创评估疾病、神经活动和胚胎发生的有力工具[141]。而在 CARS 成像中，CARS 信号通常伴随强烈的非共振背景，可以通过偏振检测[142]、频率调制[143]、非线性干涉成像[144]以及光谱分离[145]等方法对其进行抑制，从而提高 CARS 成像的对比度与信噪比。SRS 虽然没有非共振背景，但也存在交叉相位调制、双光子吸收、激发态吸收、热透镜效应等其他背景。此外，SRS 成像容易受到激光器噪声干扰。因此，通常采用平衡探测[146]、光谱调制[147]与偏振调制[148]的方案抑制 SRS 成像噪声，以提高 SRS 成像信噪比。

5 多模态非线性光学内窥镜

在活体成像研究中，通常将非线性光学成像与内窥镜技术相结合以灵活地实现活体生物表皮与内部器官的动态监测。随着光纤、微光学和微力学的进步，该领域获得飞速发展[149-150]，但仍面临着几个关键挑战：1)将具有超短脉冲宽度的激发激光束以最小损耗传输至样品端，同时能够高效收集微弱的非线性光学信号；2)在这种微型仪器中采用的激光扫描机制应该允许尺寸缩小到毫米级，并能够实现监测生物过程的快速扫描速率；3)基于微光学的非线性光学内窥镜的设计应保持较大的灵活性和紧凑的尺寸，以便利用内窥镜对内部器官进行成像。

在非线性光学内窥成像系统中，通常采用光纤实现光的远程传输与信号收集[151-153]。单模光纤(SMFs)是光学内窥系统中最常见的光纤类型，然而，SMF 的激发脉冲传递和信号收集能力有限。一方面，超短脉冲经过 SMF 的过程中，群速度色散(GVD)、自相位调制(SPM)和自陡峭效应[154]会造成光谱展宽，从而导致非线性激发效率降低和穿透深度减小[155]。另一方面，较小的纤芯尺寸和数值孔径使单模光纤在成像系统中对光学像差非常敏感，这限制了非线性信号的收集效

率。多模光纤尽管具有相对较大的数值孔径与纤芯直径，在信号收集方面性能更好，但较大的模间色散导致其多个空间模式无法聚焦到衍射极限点附近，无法产生高效的非线性激励以获得高光学分辨率。而光子晶体光纤（PCFs）的发展克服了传统光纤的局限性[156-157]，采用一种新的物理机制来引导光，打破了传统纤维中全内反射原理的限制。大模场（LMA）PCF具有较大的核心尺寸，对任何波长具有单模引导，因此显著减弱了超短脉冲传输的非线性效应，但该类型光纤的低 *NA* 导致非线性光信号的收集效率有限[158]。空心 PCF 能够实现单波长的无畸变传播，被用于TPEF 显微镜中激发光束的传播[159]，此类光纤的工作波长通常是中心波长周围的几十纳米，这使得可见的非线性光信号不能传播。因此，空芯PCF非常适用于高能超短脉冲传输，但不能用于基于单纤维的内窥镜系统，无法实现同时脉冲传输和反向信号采集。双包层光纤的出现满足了单一模式激发光的高效传播，同时非线性信号以多模模式在内包层传输[160-162]，因此双包层光纤发挥了超短脉冲传输和非线性光信号高效收集的双重作用[163-166]，LMA 纤芯被放置在微结构的内包层中，为近红外光束提供单模引导，该纤芯具有较弱的非线性效应。具有高 *NA* 和数百微米直径的内包层可使可见光和近红外波长光束以高效率传播。针对需要两束激发光的相干拉曼成像，一种新型的双芯双包层光纤被提出，用于实现泵浦和斯托克斯激光脉冲在两个纤芯中的单模传输[167-168]。

尽管光纤可以将光远程传输到给定的点，但它们必须与扫描机构结合在一起，才能在显微镜或内窥镜中形成二维图像。微型显微镜中的扫描机制可以分为两类：近端扫描和远端扫描。近端扫描和远端扫描的确定取决于扫描单元相对于激光源的位置（图 8）。近端扫描仪不必插入内窥镜狭窄的工作通道，从而实现紧凑的探头几何结构。远端扫描仪放置在靠近内窥镜探头尖端的位置，通常与单一纤维结合，提供了多功能光学设计和高分辨率的光学成像。近端扫描通常包括扫描振镜和成像纤维束[150, 169-170]，光纤束中的每根纤芯都作为点源以及成像的探测针孔[171-172]。然而，光纤束的像素化导致了有限的横向分辨率。此外，每根光纤的信号泄漏到相邻的光纤会导致成像对比度降低。在单根光纤传输的内窥系统中，光纤尖端或光纤耦合的光束通常采用压电或电磁驱动以远端扫描的方式生成二维扫描图样[173-175]。通常，两对驱动电极组成的管状压电驱动器能够以 Lissajous 模式[173]或者螺旋扫描模式[174, 176]驱动光纤尖端。此外，微机电系统（MEMS）因其体积小、功耗低、光束操作能力强等优势被用于实现内窥系统的二维扫描[177-180]。

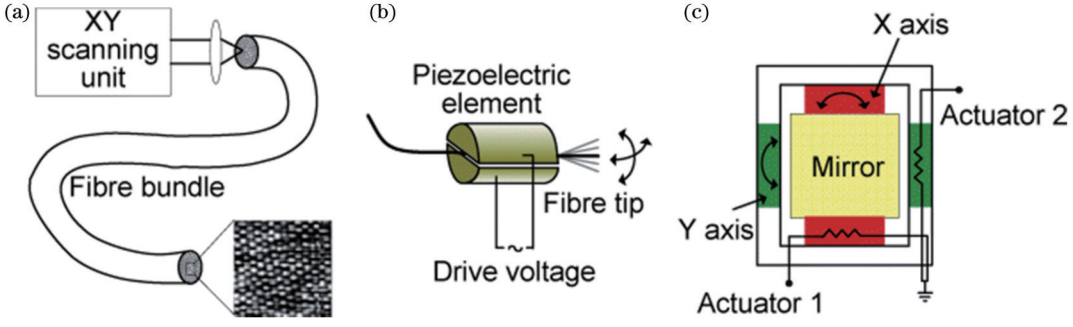

图 8 非线性光学内窥镜的扫描机制[181]。(a)结合光纤束传导的近端扫描；(b)通过压电驱动器的机械共振实现光纤尖端扫描；(c)MEMS 系统用于远端扫描

Fig. 8 Scanning mechanism of a nonlinear optical endoscope[181]. (a) Near end scanning combined with fiber bundle conduction; (b) optical fiber tip scanning is achieved through mechanical resonance of piezoelectric actuators; (c) MEMS systems are used for remote scanning

在非线性光学内窥成像中，需要通过光学设计实现尺寸紧凑并具有优良光学特性的小型化物镜。梯度折射率（GRIN）透镜尺寸通常为亚毫米，结构小巧灵活，可用于内窥成像[182-183]。与使用曲面来折射光线的传统透镜不同，GRIN 透镜使用玻璃中浓度可变的掺杂剂生成特殊的折射率剖面，使用近似抛物线形状的径向折射率剖面来引导余弦射线轨迹的光线。在实际应用中，通常将 GRIN 透镜与小尺寸透镜相结合，以进一步提高微型物镜的放大倍数、*NA*，且满足微创成像的小尺寸。

通过使用 LMA PCF、空心 PCF 和双包层 PCF 能够显著抑制或者减小超短脉冲在光纤中传输的时间展宽。特别是，双包层 PCF 可以同时实现高效的脉冲传输和非线性信号采集。同时，结合基于压电驱动器或 MEMS 的微型扫描机构以及基于 GRIN 透镜的微型物镜分别用于二维扫描以及光束聚焦，最终实现了多参量非线性光学内窥系统，图 9 展示了几种常见的多参量非线性内窥成像系统，其可实现高分辨率的活体三维成像，目前已广泛应用于深部脑组织成像和胃、食管等内脏组织成像。

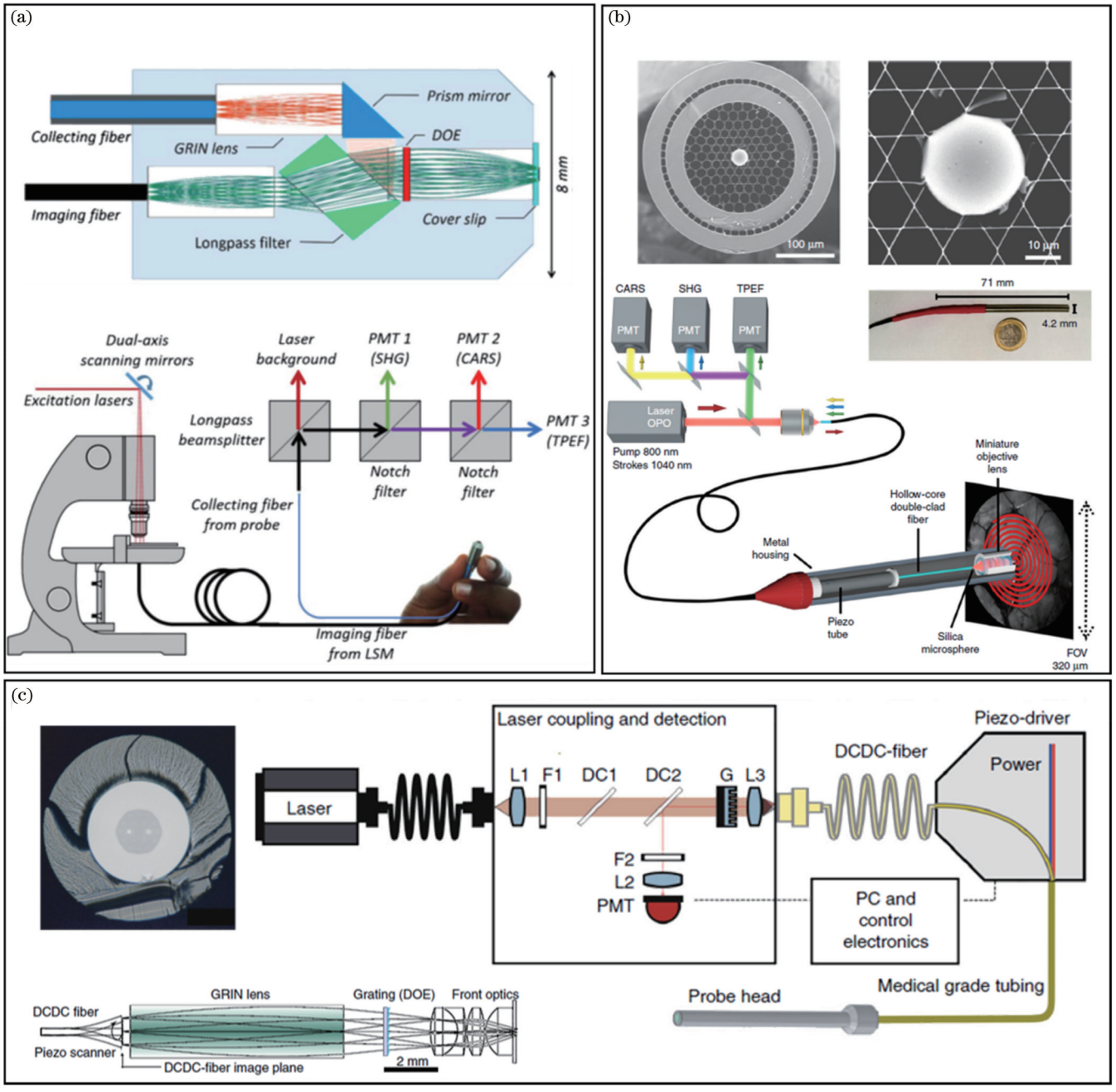

图 9　几种常见的多参量非线性内窥成像系统。(a)基于光纤束与多模光纤的近端扫描多模态光学内窥镜[170];(b)基于空心光子晶体双包层光纤与压电驱动器的远端扫描多模态光学内窥镜[131];(c)基于双芯双包层光纤与微型聚焦物镜的多模态非线性光学内窥成像系统[167]

Fig. 9　Several common multi-parameter nonlinear endoscopic imaging systems. (a) Near-end scanning multimodal optical endoscope based on fiber bundles and multimode fibers[170]; (b) remote scanning multimodal optical endoscope based on hollow photonic crystal double clad fiber and piezoelectric actuator[131]; (c) multimodal nonlinear optical endoscopic imaging system based on dual core double clad fiber and micro focusing objective[167]

6　多模态非线性光学显微成像的图像分析方法

6.1　TPEF 和 SHG 图像分析方法

非线性光学成像显微镜能够特异性可视化生物体中的组织结构与分子，但对于生物分子与组织结构的定量检测，需要结合相应的图像处理方法对成像结果进行进一步分析。在多模态非线性光学成像中，TPEF 和 SHG 成像常被用于揭示组织结构特征，尤其是组织癌变过程中上皮细胞与细胞外基质，下面描述了目前常用的图像分析方法，以量化组织中胶原纤维与弹性蛋白的组织结构、延伸方向和分布的信息，包括基于真皮二次谐波至自体荧光的衰减指数(SAAID，可用 S_{AAID} 表示)、肿瘤相关胶原特性(TACS)、快速傅

里叶变换(FFT)和灰度共生矩阵(GLCM)的方法，如图 10 所示。

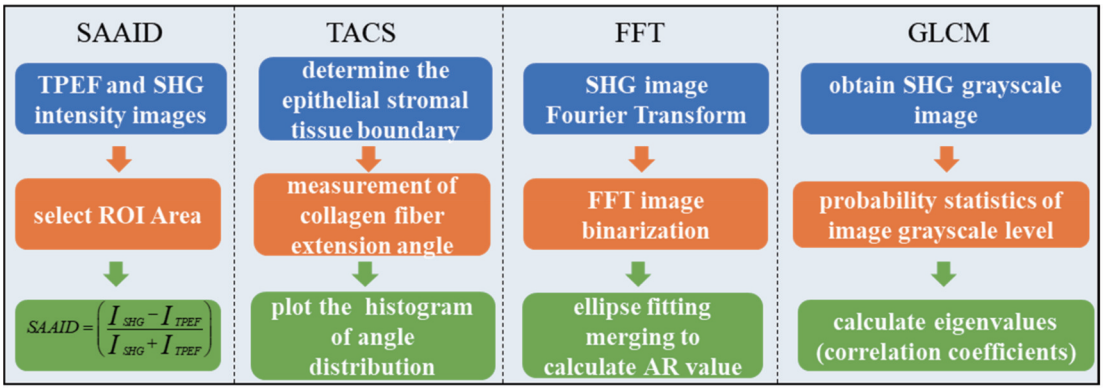

图 10　TPEF 和 SHG 图像分析方法

Fig. 10　TPEF and SHG image analysis methods

组织中细胞外基质主要由胶原纤维和弹性蛋白组成，多模态非线性光学成像中 TPEF 能够对弹性蛋白进行特异性成像，而胶原纤维具有二次谐波特性，因此，利用非线性光学信号能够区分该组织结构的病理学改变。SAAID 能够衡量基质中胶原纤维和弹性蛋白的强度比率，该指标可定义为：$S_{\mathrm{AAID}}=(I_{\mathrm{SHG}}-I_{\mathrm{TPEF}})/(I_{\mathrm{SHG}}+I_{\mathrm{TPEF}})$，其中 I_{SHG} 为二次谐波信号强度，I_{TPEF} 为双光子激发荧光信号强度[184]。具体地，首先将 TPEF 和 SHG 图像转换为 8 bit 灰度(0～255)图像类型，其次，选择基质区域作为图像感兴趣区域(ROI)，通过上述运算过程即可获得该基质区域的 SAAID 指数。上述图像分析过程可使用 ImageJ 软件实现，此外，可通过设置强度阈值的方式将非线性信号中的噪声背景与探测器暗电流分离。SAAID 评估方法可获取卵巢组织中胶原-弹性组织比值图以区分正常与卵巢癌组织[185]，此外，该方法已被证明可研究基底细胞癌真皮组织中肿瘤-基质边界的形态学改变[186-187]。

TACS 常用于确定 SHG 图像中胶原纤维相对于肿瘤-基质边界的延伸方向。在肿瘤浸润与发展的特定阶段，该参数可分为：1)TACS-1，表示在疾病早期小肿瘤周围存在密集的胶原纤维；2)TACS-2，指胶原纤维平行于上皮-基质边界排列(夹角约为 0°)；3)TACS-3，指胶原纤维平行于上皮-基质边界排列(夹角约为 90°)。采用 ImageJ 工具栏中的角度工具选项测量纤维角度，首先确定出上皮-基质边界作为基线，之后通过三个点定义胶原纤维与基线的夹角，最终通过直方图统计角度分布以确定 TACS 类型。TACS 提供了一种定量胶原纤维延伸角度的方法，被用于乳腺癌[188]、卵巢癌[67, 101]的病理特征分析。

此外，采用 FFT 方法对 SHG 图像中胶原纤维进行分析，量化表征胶原纤维的分布方向[189]。例如，沿同一方向整齐排列的胶原纤维，其 FFT 的强度图呈椭圆状，在纤维完全对齐的情况下，椭圆将坍缩为一条线。对于随机分布的胶原纤维，相应的 FFT 图像更趋近于圆。具体地，首先选择 SHG 图像特定区域进行 FFT，并对其进行二值化。进一步地，对阈值 FFT 图像进行椭圆拟合，计算其短轴与长轴的比值(AR)[190]。当 AR 趋近于 1 时，样品胶原分布表现为各向异性，而当 AR 近似于 0，胶原纤维分布具有各向同性。FFT 分析法已被用于区分正常与不同病理亚型乳腺癌以及卵巢癌组织。

GLCM 分析法能够提供给定图像中像素亮度值空间关系的信息以描述图像的纹理特征[191]。GLCM 的构造方法是，在指定的像素距离 d 处，计算其灰度值与相邻像素灰度值共同出现的频次，并将其进行归一化以获得概率。GLCM 分析采用角矩阵、对比度、逆差距、熵以及自相关等方法进行统计。其中，自相关法可度量空间灰度共生矩阵元素在行或列方向上的相似程度，因此，自相关法是应用于胶原蛋白 SHG 图像分析最有力的方法。研究显示正常卵巢组织中胶原纤维的相关性随着距离的增加而急剧降低，而卵巢癌中胶原纤维的相关性在较长的距离内保持升高，这意味着恶性肿瘤组织中胶原纤维表现出较高的复杂性和较低的组织性[192-193]。上述分析方法被广泛应用于多种类型病理组织切片的形态结构量化分析，图 11 展示了 TPEF 和 SHG 分析方法对正常卵巢与卵巢癌组织切片的胶原纤维特性的量化分析结果。

6.2　SRS 图像分析方法

SRS 显微成像技术能够实现生物体分子(脂质、蛋白质等)的成像并获得相应的拉曼光谱，高光谱 SRS 成像技术通常可以获得像素级的三维光谱图像数据栈，即空间 X-Y 和拉曼频移 Ω 数据。目前，最小二乘法、主成分分析(PCA)[194]、独立成分分析(ICA)[195]以及多元曲线分辨(MCR)[196]等被广泛用于分析处理 X-Y-Ω 图像堆栈。其中，最小二乘法适用于分子成分已知的单光谱成像，PCA 和 ICA 被用来区分样品中的关键成分。MCR 可以在主要组分的光谱未知的情况

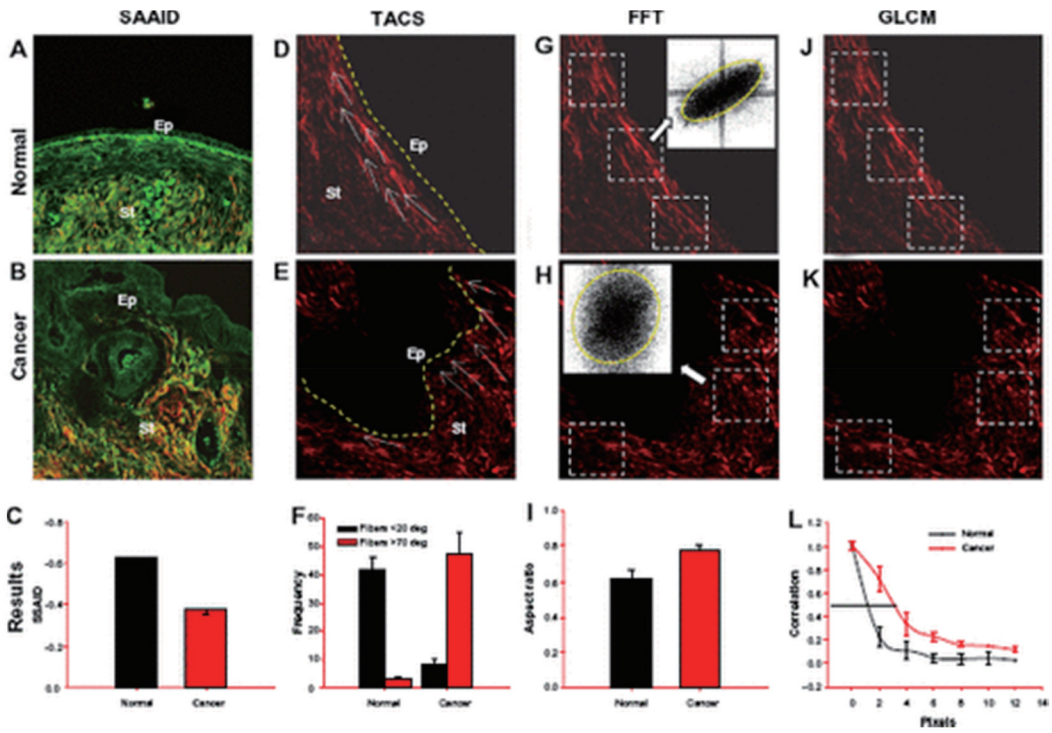

图 11　正常卵巢(A, D, G, J)与卵巢癌(B, E, H, K)组织的 TPEF 与 SHG 图像,以及正常卵巢和卵巢癌组织的 SAAID 指数(C)、TACS 统计(F)和各向异性直方图(I)以及空间关系相关性曲线(L)[185]

Fig. 11　TPEF and SHG images of normal ovarian (A, D, G, J) and ovarian cancer (B, E, H, K) tissues, and SAAID index (C), TACS statistics (F), anisotropic histogram (I), and spatial correlation curves (L) of normal ovarian and ovarian cancer tissues[185]

下,提取原始拉曼光谱并量化分子浓度,其数据处理过程如图 12 所示。首先将高光谱图像 X-Y-Ω 数据栈转换为每个像素的光谱数据二维矩阵 $\boldsymbol{D}$,该矩阵可进一步分解为 $\boldsymbol{C}$ 和 $\boldsymbol{S}^{\mathrm{T}}$ 两个矩阵的乘积:

$$\boldsymbol{D}=\boldsymbol{C}\cdot\boldsymbol{S}^{\mathrm{T}}+\boldsymbol{E}, \tag{2}$$

式中:$\boldsymbol{C}$ 为每个组分的浓度映射矩阵;$\boldsymbol{S}^{\mathrm{T}}$ 为相应的光谱矩阵;$\boldsymbol{E}$ 为误差矩阵。构成矩阵 $\boldsymbol{D}$ 的分子组分可通过 PCA 算法获得,以对光谱矩阵 $\boldsymbol{S}^{\mathrm{T}}$ 进行初步估计,并计算 $\boldsymbol{C}$ 和 $\boldsymbol{S}^{\mathrm{T}}$。在该过程中可通过交叉最小二乘法(ALS)对上述分解进行迭代优化,直至收敛。具体地,将原始 SRS 光谱数据栈展开为矩阵 $\boldsymbol{D}$,其中每一行代表不同波长下的 SRS 信号强度。然后利用 MATLAB 中的 MCR-ALS 工具箱检索各组分的浓度矩阵和光谱,以获得矩阵 $\boldsymbol{C}$ 和 $\boldsymbol{S}^{\mathrm{T}}$。最后,采用 MATLAB 和 ImageJ 对相应的图像进行重构,并输出不同分子的成像结果。

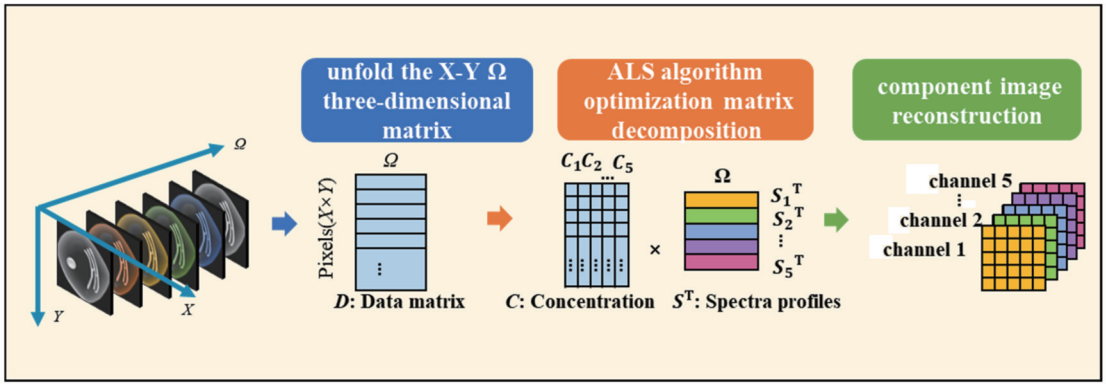

图 12　多元曲线分辨用于 SRS 图像分析

Fig. 12　Multivariate curve resolution for SRS image analysis

6.3　TP-FLIM 图像分析方法

时间分辨荧光寿命显微成像通过荧光分子寿命信息的差异获得图像对比度,被广泛应用于生命科学中,用于研究和量化离子浓度、pH 等与代谢相关的微环境变化,该方法可从另一维度对荧光团进行特异性表征。TP-FLIM 成像能够创建一个彩色映射图像,不同的颜

色代表不同的荧光寿命衰减，FLIM 成像通常采用相量图进行分析，如图 13 所示[197-201]。

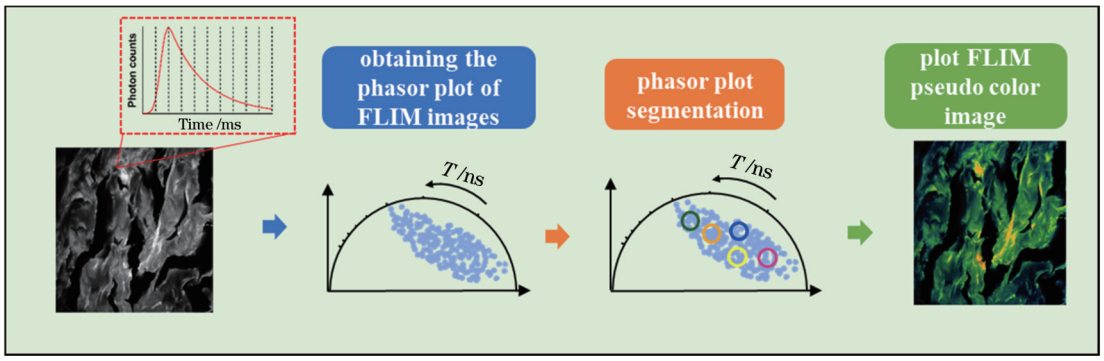

图 13　TP-FLIM 相量图分析

Fig. 13　TP-FLIM phasor diagram analysis

该方法首先对包含荧光寿命信息的 X-Y-τ 三维数据进行傅里叶变换，在时域荧光寿命探测中，时频域的对应关系[197]为

$$s_{i,j}(\omega)=\frac{\int_0^T I(t)\sin(n\omega t)\mathrm{d}t}{\int_0^T I(t)\mathrm{d}t},\tag{3}$$

$$g_{i,j}(\omega)=\frac{\int_0^T I(t)\cos(n\omega t)\mathrm{d}t}{\int_0^T I(t)\mathrm{d}t},\tag{4}$$

式中：(i,j) 为图像像素坐标；$\omega=2\pi f$ 为谐振频率，f 为激光器的重复频率；T 为采集的重复次数。而采用频域 FLIM 探测获得的数据可根据下面关系转换为相量点[198]：

$$s_{i,j}(\omega)=m_{i,j}\sin(\phi_{i,j}),\tag{5}$$

$$g_{i,j}(\omega)=m_{i,j}\cos(\phi_{i,j}),\tag{6}$$

式中：$m_{i,j}$ 和 $\phi_{i,j}$ 分别为像素位置 (i,j) 处的强度与相位解调结果。相量图是极坐标图，在笛卡儿坐标系中，每个荧光寿命都用 $g_{i,j}(\omega)$ 和 $s_{i,j}(\omega)$ 两个坐标表示。在相量图中，具有相同荧光寿命的像素聚集于同一位置，因此可以选择相量图中的任意区域（对应于某一范围的荧光寿命衰减类型）作为簇，以直接识别图中具有相同荧光寿命特征的分子或结构。在相量变换中，单指数衰减的荧光寿命分布通常出现在半圆上，其中 $g_{i,j}(\omega)$（余弦变换）的值在 0 到 1 之间，$s_{i,j}(\omega)$（正弦变换）的值在 0 到 0.5 之间，如图 14(a)所示。而多指数荧光寿命衰减出现在半圆内，如图 14(b)所示。依据相量变换中的线性叠加定律，其平均荧光寿命 τ 来源于两个相量点（即两个组分对应的荧光寿命）τ_1 和 τ_2 的贡献，其占比与距离 a_1 和 a_2 成反比。因此，基于多组分的相量图分析能够使具有相似荧光寿命衰减特征的分子在相量图中形成簇，以区分不同的荧光团分子与结构信息，并且可进一步分离样品中不同的荧光寿命组分信息。此外，荧光寿命可以通过拟合曲线的方式来获取，并利用拟合曲线参数来描述荧光寿命变化的规律。常用的荧光寿命拟合曲线模型有单指数模型、双指数模型和三指数模型等。在拟合曲线时，可以通过最小二乘法或者非线性最小二乘法来获取拟合曲线参数。根据实验数据的特点和模型的复杂程度选择合适的拟合方法和模型。

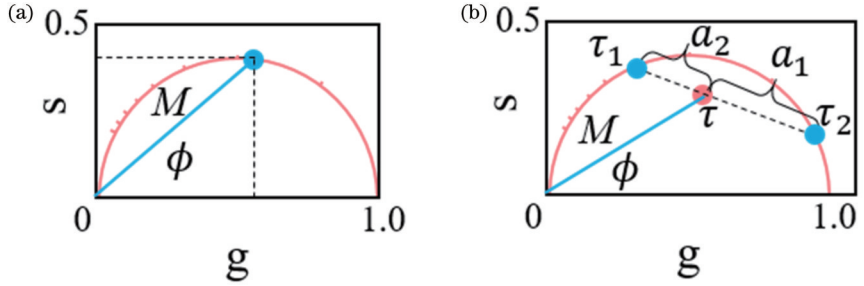

图 14　单组分与多组分荧光寿命相量图[197]。(a)单组分；(b)多组分

Fig. 14　Single component and multi-component fluorescence lifetime phasor plots[197]. (a) Single component; (b) multi-component

7　总结与展望

多模态非线性光学显微成像技术能够利用不同非线性成像对比机制对生物样进行多维光学表征成像，并具有衍射极限空间分辨率、光学切片效果、大的穿透深度、小的光损伤以及分子特异性。其中，TPEF 和

3PEF可以显示各种内源性荧光团(NADH,FAD)的分布,同时结合荧光寿命可揭示与癌症发展相关的分子代谢活动,发生在非中心对称材料和超极化生物分子中的SHG信号对胶原蛋白、微管和肌球蛋白具有特异性,THG成像能够凸显折射率突变的交界面(如间质液和组织交界处),而CRS成像能够对生物体中的生物分子(脂质、蛋白等)进行可视化和定量。将该成像技术与相应的定量分析方法结合能够从多个信息维度对生物体组织结构与生理动态过程进行成像表征,因此该技术是非线性光学显微成像发展的重要分支,被广泛应用于细胞检测[202]、癌症诊断[203-206]以及脑成像研究[207]等生物医学领域[208-210],尤其在临床病理学诊断中具有较大的潜力[83, 95, 204, 211]。但该技术仍有以下几方面需要进一步完善与提升:

1)快速的多模态非线性光学成像。目前,为了获得高对比度、高信噪比的非线性图像,大多数成像系统采用双检流镜进行二维图像扫描,其成像速度最快可达2 frame/s(512 pixel×512 pixel)。尽管采用共振扫描器、声光偏转器等装置可替代单轴检流镜来提高成像速度,但基于TCSPC的TP-FLIM成像需要较长的时间进行光子累积以获得寿命衰减曲线,同时SRS也需要改变时间延迟位移台的位置来完成光谱扫描,这两种成像方式仍旧限制着系统的成像速度,无法实现一些动态过程的多参量光学表征。在未来的发展中,可以采用频域FLIM成像[212-213]、多色SRS成像[214-215]来提高这两种模式的成像速度。此外,采用深度学习方法可打破成像速度、视场和空间分辨率之间的固有限制,有效提高系统成像速度[216]。

2)活体多模态非线性光学成像。在非线性光学成像中,TPEF、SHG和TP-FLIM成像均可采用后向探测进行信号收集,而SRS成像中后向散射信号较弱,很难收集足够用于解调出高信噪比信号的散射光,因而采用前向透射收集。这种收集方式导致该系统不适用于除鼠耳等薄组织以外的大部分活体成像以及光学内窥镜。CARS虽然有着较强的非共振背景,但可通过偏振调制等方式将其去除,相比于SRS更便于应用于活体成像和较为灵活的内窥成像。此外,在SRS信号足够强的情况下,可采用环形探测、偏振分离探测等方式实现SRS的后向探测。而CARS成像可作为备选方案,取代SRS成像作为分子振动信息的获取方式。另一方面,利用量子光子相关性可以提高非线性光学成像的信噪比[217],该方法能够解决SRS后向探测信噪比较低的问题,实现高信噪比的活体成像。

3)在实际应用中,多模态非线性光学成像系统所获得的图像需要结合相应的分析方法,通过大量的数据处理与统计分析才能获得对应的生化信息,尤其是临床病理分析。这些分析方法可被人工智能中的深度学习模型替代,以实现光学图像到生物信息的快速转换[218-223]。此外,深度学习算法也被广泛用于图像质量的提高。例如,对于信号较弱的内源性荧光团的探测,成像结果通常具有较低的信噪比,且样品散射引起的图像噪声与背景,以及SRS指纹区信号探测时信号对比度与信噪比较低等问题,均可通过人工智能算法得到进一步改善。

参 考 文 献

[1] Hellwarth R, Christensen P. Nonlinear optical microscopic examination of structure in polycrystalline ZnSe[J]. Optics Communications, 1974, 12(3): 318-322.

[2] Duncan M D, Reintjes J, Manuccia T J. Scanning coherent anti-Stokes Raman microscope[J]. Optics Letters, 1982, 7(8): 350-352.

[3] Denk W, Strickler J H, Webb W W. Two-photon laser scanning fluorescence microscopy[J]. Science, 1990, 248(4951): 73-76.

[4] Piston D W, Sandison D R, Webb W W. Time-resolved fluorescence imaging and background rejection by two-photon excitation in laser-scanning microscopy[J]. Proceedings of SPIE, 1992, 1640: 379-389.

[5] Xu C, Zipfel W, Webb W W. Three-photon excited fluorescence and applications in nonlinear laser scanning microscopy[J]. Biophysical Journal, 1996, 70(2): WP297.

[6] Ploetz E, Laimgruber S, Berner S, et al. Femtosecond stimulated Raman microscopy[J]. Applied Physics B, 2007, 87(3): 389-393.

[7] Freudiger C W, Min W, Saar B G, et al. Label-free biomedical imaging with high sensitivity by stimulated Raman scattering microscopy[J]. Science, 2008, 322(5909): 1857-1861.

[8] Gopal A A, Kazarine A, Dubach J M, et al. Recent advances in nonlinear microscopy: deep insights and polarized revelations[J]. The International Journal of Biochemistry & Cell Biology, 2021, 130: 105896.

[9] 穆书奇, 董大山, 施可彬. 无标记光学成像技术[J]. 激光与光电子学进展, 2022, 59(12): 1200001.
Mu S Q, Dong D S, Shi K B. Label-free optical imaging technology[J]. Laser & Optoelectronics Progress, 2022, 59(12): 1200001.

[10] Piston D W, Kirby M S, Cheng H P, et al. Two-photon-excitation fluorescence imaging of three-dimensional calcium-ion activity[J]. Applied Optics, 1994, 33(4): 662-669.

[11] Patterson G H, Knobel S M, Arkhammar P, et al. Separation of the glucose-stimulated cytoplasmic and mitochondrial NAD(P)H responses in pancreatic islet beta cells[J]. Proceedings of the National Academy of Sciences of the United States of America, 2000, 97(10): 5203-5207.

[12] Huang S H, Heikal A A, Webb W W. Two-photon fluorescence spectroscopy and microscopy of NAD(P)H and flavoprotein[J]. Biophysical Journal, 2002, 82(5): 2811-2825.

[13] Deyl Z, Macek K, Adam M, et al. Studies on the chemical nature of elastin fluorescence[J]. Biochimica et Biophysica Acta (BBA) - Protein Structure, 1980, 625(2): 248-254.

[14] Gusachenko I, Tran V, Houssen Y G, et al. Polarization-resolved second-harmonic generation in tendon upon mechanical stretching[J]. Biophysical Journal, 2012, 102(9): 2220-2229.

[15] Débarre D, Supatto W, Pena A M, et al. Imaging lipid bodies in cells and tissues using third-harmonic generation microscopy[J]. Nature Methods, 2006, 3(1): 47-53.

[16] Wang H W, Le T T, Cheng J X. Label-free imaging of arterial cells and extracellular matrix using a multimodal CARS microscope[J]. Optics Communications, 2008, 281(7): 1813-1822.

[17] Wang H F, Fu Y, Shi R Y, et al. Molecular imaging of central nervous system with multi-modal nonlinear optical microscopy

[C]//2007 Conference on Lasers and Electro-Optics (CLEO), May 6-11, 2007, Baltimore, MD, USA. New York: IEEE Press, 2008.

[18] Wang H W, Langohr I M, Sturek M, et al. Imaging and quantitative analysis of atherosclerotic lesions by CARS-based multimodal nonlinear optical microscopy[J]. Arteriosclerosis, Thrombosis, and Vascular Biology, 2009, 29(9): 1342-1348.

[19] Ko A C T, Ridsdale A, Smith M S D, et al. Multimodal nonlinear optical imaging of atherosclerotic plaque development in myocardial infarction-prone rabbits[J]. Journal of Biomedical Optics, 2010, 15(2): 020501.

[20] Murugkar S, Smith B, Srivastava P, et al. Miniaturized multimodal CARS microscope based on MEMS scanning and a single laser source[J]. Optics Express, 2010, 18(23): 23796-23804.

[21] Li D, Zheng W, Zeng Y, et al. *In vivo* and simultaneous multimodal imaging: integrated multiplex coherent anti-Stokes Raman scattering and two-photon microscopy[J]. Applied Physics Letters, 2010, 97(22): 223702.

[22] Li X S, Lam W J, Cao Z, et al. Integrated femtosecond stimulated Raman scattering and two-photon fluorescence imaging of subcellular lipid and vesicular structures[J]. Journal of Biomedical Optics, 2015, 20(11): 110501.

[23] Crisafi F, Kumar V, Perri A, et al. Multimodal nonlinear microscope based on a compact fiber-format laser source[J]. Spectrochimica Acta Part A: Molecular and Biomolecular Spectroscopy, 2018, 188: 135-140.

[24] Tserevelakis G J, Psycharakis S, Resan B, et al. Femtosecond laser nanosurgery of sub-cellular structures in HeLa cells by employing third harmonic generation imaging modality as diagnostic tool[J]. Journal of Biophotonics, 2012, 5(2): 200-207.

[25] Mouras R, Bagnaninchi P O, Downes A R, et al. Label-free assessment of adipose-derived stem cell differentiation using coherent anti-Stokes Raman scattering and multiphoton microscopy[J]. Journal of Biomedical Optics, 2012, 17(11): 116011.

[26] Lin J, Teh S, Zheng W, et al. Multimodal nonlinear optical microscopic imaging provides new insights into acetowhitening mechanisms in live mammalian cells without labeling[J]. Biomedical Optics Express, 2014, 5(9): 3116-3122.

[27] Tian Y, Kong Y, Li X J, et al. Light- and pH-activated intracellular drug release from polymeric mesoporous silica nanoparticles[J]. Colloids and Surfaces B: Biointerfaces, 2015, 134: 147-155.

[28] Tolstik E, Osminkina L A, Akimov D, et al. Linear and nonlinear optical imaging of cancer cells with silicon nanoparticles[J]. International Journal of Molecular Sciences, 2016, 17(9): 1536.

[29] Adur J, Pelegati V B, Costa L F L, et al. Recognition of serous ovarian tumors in human samples by multimodal nonlinear optical microscopy[J]. Journal of Biomedical Optics, 2011, 16(9): 096017.

[30] Bianchi M, Adur J, Ruff S Y, et al. Mouse colorectal cancer an early detection approach using nonlinear microscopy[J]. Bio-Medical Materials and Engineering, 2014, 24(6): 3419-3426.

[31] Galli R, Sablinskas V, Dasevicius D, et al. Non-linear optical microscopy of kidney tumours[J]. Journal of Biophotonics, 2014, 7(1/2): 23-27.

[32] Mouras R, Bagnaninchi P, Downes A, et al. Multimodal, label-free nonlinear optical imaging for applications in biology and biomedical science[J]. Journal of Raman Spectroscopy, 2013, 44(10): 1373-1378.

[33] Bocklitz T W, Salah F S, Vogler N, et al. Pseudo-HE images derived from CARS/TPEF/SHG multimodal imaging in combination with Raman-spectroscopy as a pathological screening tool[J]. BMC Cancer, 2016, 16(1): 1-11.

[34] Medyukhina A, Meyer T, Schmitt M, et al. Towards automated segmentation of cells and cell nuclei in nonlinear optical microscopy[J]. Journal of Biophotonics, 2012, 5(11/12): 878-888.

[35] Romeike B F M, Meyer T, Reichart R, et al. Coherent anti-Stokes Raman scattering and two photon excited fluorescence for neurosurgery[J]. Clinical Neurology and Neurosurgery, 2015, 131: 42-46.

[36] Yue S H, Slipchenko M N, Cheng J X. Multimodal nonlinear optical microscopy[J]. Laser & Photonics Reviews, 2011, 5(4): 496-512.

[37] Suhling K, Hirvonen L M, Levitt J A, et al. Fluorescence lifetime imaging (FLIM): basic concepts and some recent developments[J]. Medical Photonics, 2015, 27: 3-40.

[38] Poudel C, Mela I, Kaminski C F. High-throughput, multi-parametric, and correlative fluorescence lifetime imaging[J]. Methods and Applications in Fluorescence, 2020, 8(2): 024005.

[39] Kleinman D A. Theory of second harmonic generation of light [J]. Physical Review, 1962, 128(4): 1761-1775.

[40] Rosen P. Generation of the third harmonic by an electromagnetic signal in a plasma[J]. The Physics of Fluids, 1961, 4(3): 341-345.

[41] Roth S, Freund I. Second harmonic generation in collagen[J]. The Journal of Chemical Physics, 1979, 70(4): 1637-1643.

[42] Campagnola P J, Millard A C, Terasaki M, et al. Three-dimensional high-resolution second-harmonic generation imaging of endogenous structural proteins in biological tissues[J]. Biophysical Journal, 2002, 82(1): 493-508.

[43] Perrenoud-Rinuy J, Brevet P F, Girault H H. Second harmonic generation study of myoglobin and hemoglobin and their protoporphyrin IX chromophore at the water/1, 2-dichloroethane interface[J]. Physical Chemistry Chemical Physics, 2002, 4(19): 4774-4781.

[44] Sun Y, You S, Du X, et al. Real-time three-dimensional histology-like imaging by label-free nonlinear optical microscopy [J]. Quantitative Imaging in Medicine and Surgery, 2020, 10(11): 2177-2190.

[45] Farrar M J, Wise F W, Fetcho J R, et al. *In vivo* imaging of myelin in the vertebrate central nervous system using third harmonic generation microscopy[J]. Biophysical Journal, 2011, 100(5): 1362-1371.

[46] Lin X M, Li X H, Zhang Y B, et al. Third harmonic generation on silicon surface induced by femtosecond laser[J]. Optics & Laser Technology, 2019, 111: 255-261.

[47] Genthial R, Beaurepaire E, Schanne-Klein M C, et al. Label-free imaging of bone multiscale porosity and interfaces using third-harmonic generation microscopy[J]. Scientific Reports, 2017(1), 7: 3419.

[48] Wei L, Yu Y, Shen Y H, et al. Vibrational imaging of newly synthesized proteins in live cells by stimulated Raman scattering microscopy[J]. Proceedings of the National Academy of Sciences of the United States of America, 2013, 110(28): 11226-11231.

[49] Shen Y H, Xu F, Wei L, et al. Live-cell quantitative imaging of proteome degradation by stimulated Raman scattering[J]. Angewandte Chemie International Edition, 2014, 53(22): 5596-5599.

[50] Hong S L, Chen T, Zhu Y T, et al. Live-cell stimulated Raman scattering imaging of alkyne-tagged biomolecules[J]. Angewandte Chemie International Edition, 2014, 53(23): 5827-5831.

[51] Wei L, Hu F H, Shen Y H, et al. Live-cell imaging of alkyne-tagged small biomolecules by stimulated Raman scattering[J]. Nature Methods, 2014, 11(4): 410-412.

[52] Hu F H, Zeng C, Long R, et al. Supermultiplexed optical imaging and barcoding with engineered polyynes[J]. Nature Methods, 2018, 15(3): 194-200.

[53] Barad Y, Eisenberg H, Horowitz M, et al. Nonlinear scanning laser microscopy by third harmonic generation[J]. Applied Physics Letters, 1997, 70(8): 922-924.

[54] van Huizen L M G, Radonic T, van Mourik F, et al. Compact portable multiphoton microscopy reveals histopathological hallmarks of unprocessed lung tumor tissue in real time[J]. Translational Biophotonics, 2020, 2(4): e202000009.

[55] Mahou P, Olivier N, Labroille G, et al. Combined third-harmonic generation and four-wave mixing microscopy of tissues and embryos[J]. Biomedical Optics Express, 2011, 2(10): 2837-2849.

[56] Aptel F, Olivier N, Deniset-Besseau A, et al. Multimodal nonlinear imaging of the human cornea[J]. Investigative Opthalmology & Visual Science, 2010, 51(5): 2459-2465.

[57] Barton J K, Amirsolaimani B, Rice P, et al. Three-photon imaging of ovarian cancer[J]. Proceedings of SPIE, 2016, 9689: 96893P.

[58] Mouras R, Rischitor G, Downes A, et al. Nonlinear optical microscopy for drug delivery monitoring and cancer tissue imaging[J]. Journal of Raman Spectroscopy, 2010, 41(8): 848-852.

[59] Chung H Y, Greinert R, Glatzel M, et al. Label-free multiphoton microscopy in human tissue enabled by an Er: fiber-laser based tunable source[C]//2019 Conference on Lasers and Electro-Optics Europe & European Quantum Electronics Conference (CLEO/Europe-EQEC), June 23-27, 2019, Munich, Germany. New York: IEEE Press, 2019.

[60] Buurman E P, Sanders R, Draaijer A, et al. Fluorescence lifetime imaging using a confocal laser scanning microscope[J]. Scanning, 1992, 14(3): 155-159.

[61] Becker W. Fluorescence lifetime imaging: techniques and applications[J]. Journal of Microscopy, 2012, 247(2): 119-136.

[62] Schlachter S, Elder A D, Esposito A, et al. MhFLIM: resolution of heterogeneous fluorescence decays in widefield lifetime microscopy[J]. Optics Express, 2009, 17(3): 1557-1570.

[63] Chen H T, Gratton E. A practical implementation of multifrequency widefield frequency-domain fluorescence lifetime imaging microscopy[J]. Microscopy Research and Technique, 2013, 76(3): 282-289.

[64] Shen B L, Yan J S, Wang S Q, et al. Label-free whole-colony imaging and metabolic analysis of metastatic pancreatic cancer by an autoregulating flexible optical system[J]. Theranostics, 2020, 10(4): 1849-1860.

[65] Wang S Q, Li Y P, Zhao Y H, et al. Investigating tunneling nanotubes in ovarian cancer based on two-photon excitation FLIM-FRET[J]. Biomedical Optics Express, 2021, 12(4): 1962-1973.

[66] Lin F R, Zhang C S, Li Y P, et al. Human serum albumin gradient in serous ovarian cancer cryosections measured by fluorescence lifetime[J]. Biomedical Optics Express, 2021, 12(3): 1195-1204.

[67] Yan J S, Zhao Y H, Lin F R, et al. Monitoring the extracellular matrix remodeling of high-grade serous ovarian cancer with nonlinear optical microscopy[J]. Journal of Biophotonics, 2021, 14(6): e202000498.

[68] Li Y P, Shen B L, Zou G J, et al. Fast denoising and lossless spectrum extraction in stimulated Raman scattering microscopy [J]. Journal of Biophotonics, 2021, 14(8): e202100080.

[69] Mouras R, Downes A, Rischitor G, et al. A multimodal multiphoton microscope for biological imaging[J]. Proceedings of SPIE, 2010, 7569: 756933.

[70] Svedberg F, Brackmann C, Hellerer T, et al. Nonlinear microscopy with fiber laser continuum excitation[J]. Journal of Biomedical Optics, 2010, 15(2): 026026.

[71] Cheng J X, Jia Y K, Zheng G F, et al. Laser-scanning coherent anti-Stokes Raman scattering microscopy and applications to cell biology[J]. Biophysical Journal, 2002, 83(1): 502-509.

[72] Chen H T, Wang H F, Slipchenko M N, et al. A multimodal platform for nonlinear optical microscopy and microspectroscopy [J]. Optics Express, 2009, 17(3): 1282-1290.

[73] Pegoraro A F, Slepkov A D, Ridsdale A, et al. Single laser source for multimodal coherent anti-Stokes Raman scattering microscopy[J]. Applied Optics, 2010, 49(25): F10-F17.

[74] Fu Y, Wang H F, Shi R Y, et al. Second harmonic and sum frequency generation imaging of fibrous astroglial filaments in *ex vivo* spinal tissues[J]. Biophysical Journal, 2007, 92(9): 3251-3259.

[75] Langbein W, Rocha-Mendoza I, Borri P. Single source coherent anti-Stokes Raman microspectroscopy using spectral focusing[J]. Applied Physics Letters, 2009, 95(8): 081109.

[76] Hellerer T, Enejder A M K, Zumbusch A. Spectral focusing: high spectral resolution spectroscopy with broad-bandwidth laser pulses[J]. Applied Physics Letters, 2004, 85(1): 25-27.

[77] Lu F K, Zheng W, Lin J, et al. Integrated coherent anti-Stokes Raman scattering and multiphoton microscopy for biomolecular imaging using spectral filtering of a femtosecond laser[J]. Applied Physics Letters, 2010, 96(13): 133701.

[78] Cheng J X, Volkmer A, Xie X S. Theoretical and experimental characterization of coherent anti-Stokes Raman scattering microscopy[J]. Journal of the Optical Society of America B, 2002, 19(6): 1363-1375.

[79] Volkmer A, Cheng J X, Sunney Xie X. Vibrational imaging with high sensitivity via epidetected coherent anti-stokes Raman scattering microscopy[J]. Physical Review Letters, 2001, 87(2): 023901.

[80] Moreaux L, Sandre O, Charpak S, et al. Coherent scattering in multi-harmonic light microscopy[J]. Biophysical Journal, 2001, 80(3): 1568-1574.

[81] Huff T B, Shi Y Z, Fu Y, et al. Multimodal nonlinear optical microscopy and applications to central nervous system imaging [J]. IEEE Journal of Selected Topics in Quantum Electronics, 2008, 14(1): 4-9.

[82] Tu H H, Liu Y, Turchinovich D, et al. Stain-free histopathology by programmable supercontinuum pulses[J]. Nature Photonics, 2016, 10(8): 534-540.

[83] You S X, Tu H H, Chaney E J, et al. Intravital imaging by simultaneous label-free autofluorescence-multiharmonic microscopy[J]. Nature Communications, 2018, 9: 2125.

[84] Sowa M G, Mostaco-Guidolin L B, Smith M S D, et al. Nonlinear optical measurements of the artery wall: parameters related to the progression of atherosclerosis[J]. Measurement Science Review, 2009, 9(4): 93-94.

[85] Meyer T, Baumgartl M, Gottschall T, et al. A compact microscope setup for multimodal nonlinear imaging in clinics and its application to disease diagnostics[J]. Analyst, 2013, 138(14): 4048-4057.

[86] Meyer T, Chemnitz M, Baumgartl M, et al. Expanding multimodal microscopy by high spectral resolution coherent anti-Stokes Raman scattering imaging for clinical disease diagnostics [J]. Analytical Chemistry, 2013, 85(14): 6703-6715.

[87] Lee E S, Park J H, Lee S W, et al. Lipid crystals mechanically stimulate adjacent extracellular matrix in advanced atherosclerotic plaques[J]. Atherosclerosis, 2014, 237(2): 769-776.

[88] You S, Chaney E J, Tu H, et al. Label-free deep profiling of the tumor microenvironment[J]. Cancer Research, 2021, 81(9): 2534-2544.

[89] Liu Y A, Tu H H, You S X, et al. Label-free molecular profiling for identification of biomarkers in carcinogenesis using multimodal multiphoton imaging[J]. Quantitative Imaging in Medicine and Surgery, 2019, 9(5): 742.

[90] Lin J, Lu F K, Zheng W, et al. Assessment of liver steatosis and fibrosis in rats using integrated coherent anti-Stokes Raman scattering and multiphoton imaging technique[J]. Journal of Biomedical Optics, 2011, 16(11): 116024.

[91] Meyer T, Guntinas-Lichius O, von Eggeling F, et al. Multimodal nonlinear microscopic investigations on head and

neck squamous cell carcinoma: toward intraoperative imaging[J]. Head & Neck, 2013, 35(9): E280-E287.

[92] Heuke S, Vogler N, Meyer T, et al. Multimodal mapping of human skin[J]. British Journal of Dermatology, 2013, 169(4): 794-803.

[93] Nandakumar P, Kovalev A, Volkmer A. Vibrational imaging based on stimulated Raman scattering microscopy[J]. New Journal of Physics, 2009, 11(3): 033026.

[94] Slipchenko M N, Chen H T, Ely D R, et al. Vibrational imaging of tablets by epi-detected stimulated Raman scattering microscopy[J]. Analyst, 2010, 135(10): 2613-2619.

[95] Zou F, Zhang L L, Zou X, et al. Differential characterization of lumbar spine associated tissue histology with nonlinear optical microscopy[J]. Biomedical Optics Express, 2021, 13(1): 474-484.

[96] Zhang B, Xu H, Chen J, et al. Highly specific and label-free histological identification of microcrystals in fresh human gout tissues with stimulated Raman scattering[J]. Theranostics, 2021, 11(7): 3074-3088.

[97] He S C, Ye C, Sun Q Q, et al. Label-free nonlinear optical imaging of mouse retina[J]. Biomedical Optics Express, 2015, 6(3): 1055-1066.

[98] Li R, Wang X X, Zhou Y, et al. Advances in nonlinear optical microscopy for biophotonics[J]. Journal of Nanophotonics, 2018, 12(3): 033007.

[99] Janghyuk L, Rachel H, Nuccio E E, et al. Label-free multiphoton imaging of microbes in root, mineral, and soil matrices with time-gated coherent Raman and fluorescence lifetime imaging[J]. Environmental Science & Technology, 2022, 56(3): 1994-2008.

[100] Chrabaszcz K, Meyer T, Bae H, et al. Comparison of standard and HD FT-IR with multimodal CARS/TPEF/SHG/FLIMS imaging in the detection of the early stage of pulmonary metastasis of murine breast cancer[J]. The Analyst, 2020, 145(14): 4982-4990.

[101] Li Y P, Shen B L, Zou G J, et al. Super-multiplex nonlinear optical imaging unscrambles the statistical complexity of cancer subtypes and tumor microenvironment[J]. Advanced Science, 2022, 9(5): e2104379.

[102] Li Y P, Shen B L, Lu Y, et al. Multidimensional quantitative characterization of the tumor microenvironment by multicontrast nonlinear microscopy[J]. Biomedical Optics Express, 2022, 13(10): 5517-5532.

[103] Sacconi L, Ferrantini C, Lotti J, et al. Action potential propagation in transverse-axial tubular system is impaired in heart failure[J]. Proceedings of the National Academy of Sciences of the United States of America, 2012, 109(15): 5815-5819.

[104] Duemani Reddy G, Kelleher K, Fink R, et al. Three-dimensional random access multiphoton microscopy for functional imaging of neuronal activity[J]. Nature Neuroscience, 2008, 11(6): 713-720.

[105] Lee S, Vinegoni C, Feruglio P F, et al. Real-time *in vivo* imaging of the beating mouse heart at microscopic resolution[J]. Nature Communications, 2012, 3: 1054.

[106] Bélanger E, Bégin S, Laffray S, et al. Quantitative myelin imaging with coherent anti-Stokes Raman scattering microscopy: alleviating the excitation polarization dependence with circularly polarized laser beams[J]. Optics Express, 2009, 17(21): 18419-18432.

[107] Huff T B, Shi Y Z, Sun W J, et al. Real-time CARS imaging reveals a calpain-dependent pathway for paranodal myelin retraction during high-frequency stimulation[J]. PLoS One, 2011, 6(3): e17176.

[108] Tai D C S, Tan N, Xu S Y, et al. Fibro-C-Index: comprehensive, morphology-based quantification of liver fibrosis using second harmonic generation and two-photon microscopy [J]. Journal of Biomedical Optics, 2009, 14(4): 044013.

[109] You S X, Barkalifa R, Chaney E J, et al. Label-free visualization and characterization of extracellular vesicles in breast cancer[J]. Proceedings of the National Academy of Sciences of the United States of America, 2019, 116(48): 24012-24018.

[110] So P T C, Yew E Y S, Rowlands C. High-throughput nonlinear optical microscopy[J]. Biophysical Journal, 2013, 105(12): 2641-2654.

[111] König K, So P T C, Mantulin W W, et al. Cellular response to near-infrared femtosecond laser pulses in two-photon microscopes[J]. Optics Letters, 1997, 22(2): 135-136.

[112] Kim K H, Buehler C, So P T C. High-speed, two-photon scanning microscope[J]. Applied Optics, 1999, 38(28): 6004-6009.

[113] Iyer V, Hoogland T M, Saggau P. Fast functional imaging of single neurons using random-access multiphoton (RAMP) microscopy[J]. Journal of Neurophysiology, 2006, 95(1): 535-545.

[114] Kirkby P A, Srinivas Nadella K M S, Silver R A. A compact acousto-optic lens for 2D and 3D femtosecond based 2-photon microscopy[J]. Optics Express, 2010, 18(13): 13721-13745.

[115] Evans C L, Potma E O, Puoris'haag M, et al. Chemical imaging of tissue *in vivo* with video-rate coherent anti-Stokes Raman scattering microscopy[J]. Proceedings of the National Academy of Sciences of the United States of America, 2005, 102(46): 16807-16812.

[116] Saar B G, Freudiger C W, Reichman J, et al. Video-rate molecular imaging *in vivo* with stimulated Raman scattering[J]. Science, 2010, 330(6009): 1368-1370.

[117] Buist A H, Müller M, Squier J, et al. Real time two-photon absorption microscopy using multi point excitation[J]. Journal of Microscopy, 1998, 192(2): 217-226.

[118] Kim K H, Buehler C, Bahlmann K, et al. Multifocal multiphoton microscopy based on multianode photomultiplier tubes[J]. Optics Express, 2007, 15(18): 11658-11678.

[119] Nielsen T, Fricke M, Hellweg D, et al. High efficiency beam splitter for multifocal multiphoton microscopy[J]. Journal of Microscopy, 2001, 201(3): 368-376.

[120] Sacconi L, Froner E, Antolini R, et al. Multiphoton multifocal microscopy exploiting a diffractive optical element[J]. Optics Letters, 2003, 28(20): 1918-1920.

[121] Choi H, Tzeranis D S, Cha J W, et al. 3D-resolved fluorescence and phosphorescence lifetime imaging using temporal focusing wide-field two-photon excitation[J]. Optics Express, 2012, 20(24): 26219-26235.

[122] Goda K, Tsia K K, Jalali B. Serial time-encoded amplified imaging for real-time observation of fast dynamic phenomena[J]. Nature, 2009, 458(7242): 1145-1149.

[123] Premadasa U I, Bible A N, Morrell-Falvey J L, et al. Spatially co-registered wide-field nonlinear optical imaging of living and complex biosystems in a total internal reflection geometry[J]. The Analyst, 2021, 146(9): 3062-3072.

[124] 刘智, 罗泽伟, 王正印, 等. 基于结构照明的超分辨荧光显微成像重建算法[J]. 中国激光, 2021, 48(3): 0307001.
Liu Z, Luo Z W, Wang Z Y, et al. Super-resolution fluorescence microscopy image reconstruction algorithm based on structured illumination[J]. Chinese Journal of Lasers, 2021, 48(3): 0307001.

[125] Ding J B, Takasaki K T, Sabatini B L. Supraresolution imaging in brain slices using stimulated-emission depletion two-photon laser scanning microscopy[J]. Neuron, 2009, 63(4): 429-437.

[126] Huang B, Babcock H, Zhuang X W. Breaking the diffraction barrier: super-resolution imaging of cells[J]. Cell, 2010, 143(7): 1047-1058.

[127] Schermelleh L, Heintzmann R, Leonhardt H. A guide to super-resolution fluorescence microscopy[J]. The Journal of Cell

Biology, 2010, 190(2): 165-175.
[128] Bethge P, Chéreau R, Avignone E, et al. Two-photon excitation STED microscopy in two colors in acute brain slices [J]. Biophysical Journal, 2013, 104(4): 778-785.
[129] Isobe K, Takeda T, Mochizuki K, et al. Enhancement of lateral resolution and optical sectioning capability of two-photon fluorescence microscopy by combining temporal-focusing with structured illumination[J]. Biomedical Optics Express, 2013, 4 (11): 2396-2410.
[130] Upputuri P K, Wu Z, Gong L, et al. Super-resolution coherent anti-Stokes Raman scattering microscopy with photonic nanojets [J]. Optics Express, 2014, 22(11): 12890-12899.
[131] Lombardini A, Mytskaniuk V, Sivankutty S, et al. High-resolution multimodal flexible coherent Raman endoscope[J]. Light: Science & Applications, 2018, 7: 10.
[132] Gong L, Wang H F. Breaking the diffraction limit by saturation in stimulated-Raman-scattering microscopy: a theoretical study [J]. Physical Review A, 2014, 90(1): 013818.
[133] Gong L, Wang H F. Suppression of stimulated Raman scattering by an electromagnetically-induced-transparency-like scheme and its application for super-resolution microscopy[J]. Physical Review A, 2015, 92(2): 023828.
[134] Kim D, Choi D S, Kwon J, et al. Selective suppression of stimulated Raman scattering with another competing stimulated Raman scattering[J]. The Journal of Physical Chemistry Letters, 2017, 8(24): 6118-6123.
[135] Rao B J, Cho M. Three-beam double stimulated Raman scatterings: cascading configuration[J]. The Journal of Chemical Physics, 2018, 148(11): 114201.
[136] Silva W R, Graefe C T, Frontiera R R. Toward label-free super-resolution microscopy[J]. ACS Photonics, 2016, 3(1): 79-86.
[137] Ao J P, Fang X F, Miao X C, et al. Switchable stimulated Raman scattering microscopy with photochromic vibrational probes[J]. Nature Communications, 2021, 12: 3089.
[138] Shou J W, Ozeki Y. Photoswitchable stimulated Raman scattering spectroscopy and microscopy[J]. Optics Letters, 2021, 46(9): 2176-2179.
[139] Shou J W, Komazawa A, Wachi Y, et al. Super-resolution vibrational imaging based on photoswitchable Raman probe[J]. Science Advances, 2023, 9(24): eade9118.
[140] Jang H, Li Y J, Fung A A, et al. Super-resolution SRS microscopy with A-PoD[J]. Nature Methods, 2023, 20(3): 448-458.
[141] Shen B L, Liu S W, Li Y P, et al. Deep learning autofluorescence-harmonic microscopy[J]. Light: Science & Applications, 2022, 11: 76.
[142] Cheng J X, Book L D, Xie X S. Polarization coherent anti-Stokes Raman scattering microscopy[J]. Optics Letters, 2001, 26(17): 1341-1343.
[143] Ganikhanov F, Evans C L, Saar B G, et al. High-sensitivity vibrational imaging with frequency modulation coherent anti-Stokes Raman scattering (FM CARS) microscopy[J]. Optics Letters, 2006, 31(12): 1872-1874.
[144] Marks D L, Boppart S A. Nonlinear interferometric vibrational imaging[J]. Physical Review Letters, 2004, 92(12): 123905.
[145] Liu Y X, Lee Y J, Cicerone M T. Broadband CARS spectral phase retrieval using a time-domain Kramers-Kronig transform [J]. Optics Letters, 2009, 34(9): 1363-1365.
[146] Freudiger C W, Yang W L, Holtom G R, et al. Stimulated Raman scattering microscopy with a robust fibre laser source[J]. Nature Photonics, 2014, 8(2): 153-159.
[147] Zhang D L, Slipchenko M N, Leaird D E, et al. Spectrally modulated stimulated Raman scattering imaging with an angle-to-wavelength pulse shaper[J]. Optics Express, 2013, 21(11): 13864-13874.
[148] Andreana M, Houle M A, Moffatt D J, et al. Amplitude and polarization modulated hyperspectral stimulated Raman scattering microscopy[J]. Optics Express, 2015, 23(22): 28119-28131.
[149] Mehta A D, Jung J C, Flusberg B A, et al. Fiber optic *in vivo* imaging in the mammalian nervous system[J]. Current Opinion in Neurobiology, 2004, 14(5): 617-628.
[150] Flusberg B A, Cocker E D, Piyawattanametha W, et al. Fiber-optic fluorescence imaging[J]. Nature Methods, 2005, 2(12): 941-950.
[151] Gu M, Sheppard C J R, Gan X. Image formation in a fiber-optical confocal scanning microscope[J]. Journal of the Optical Society of America A, 1991, 8(11): 1755-1761.
[152] Rouse A R, Kano A, Udovich J A, et al. Design and demonstration of a miniature catheter for a confocal microendoscope[J]. Applied Optics, 2004, 43(31): 5763-5771.
[153] Oh G, Chung E, Yun S H. Optical fibers for high-resolution *in vivo* microendoscopic fluorescence imaging[J]. Optical Fiber Technology, 2013, 19(6): 760-771.
[154] Singh S, Bradley L T. Three-photon absorption in napthalene crystals by laser excitation[J]. Physical Review Letters, 1964, 12 (22): 612-614.
[155] Bird D, Gu M. Fibre-optic two-photon scanning fluorescence microscopy[J]. Journal of Microscopy, 2002, 208(1): 35-48.
[156] Russell P. Photonic crystal fibers[J]. Science, 2003, 299(5605): 358-362.
[157] Knight J C. Photonic crystal fibres[J]. Nature, 2003, 424(6950): 847-851.
[158] Ouzounov D G, Moll K D, Foster M A, et al. Delivery of nanojoule femtosecond pulses through large-core microstructured fibers[J]. Optics Letters, 2002, 27(17): 1513-1515.
[159] Göbel W, Nimmerjahn A, Helmchen F. Distortion-free delivery of nanojoule femtosecond pulses from a Ti∶sapphire laser through a hollow-core photonic crystal fiber[J]. Optics Letters, 2004, 29 (11): 1285-1287.
[160] Liang W X, Hall G, Messerschmidt B, et al. Nonlinear optical endomicroscopy for label-free functional histology *in vivo*[J]. Light: Science & Applications, 2017, 6(11): e17082.
[161] Guan H H, Liang W X, Li A, et al. Multicolor fiber-optic two-photon endomicroscopy for brain imaging[J]. Optics Letters, 2021, 46(5): 1093-1096.
[162] Rivera D R, Brown C M, Ouzounov D G, et al. Multifocal multiphoton endoscope[J]. Optics Letters, 2012, 37(8): 1349-1351.
[163] Ye J Y, Myaing M T, Thomas T P, et al. Development of a double-clad photonic-crystal-fiber-based scanning microscope[J]. Proceedings of SPIE, 2005, 5700: 23-27.
[164] Fu L, Gan X S, Gu M. Nonlinear optical microscopy based on double-clad photonic crystal fibers[J]. Optics Express, 2005, 13 (14): 5528-5534.
[165] Myaing M T, Ye J Y, Norris T B, et al. Enhanced two-photon biosensing with double-clad photonic crystal fibers[J]. Optics Letters, 2003, 28(14): 1224-1226.
[166] Brustlein S, Berto P, Hostein R, et al. Double-clad hollow core photonic crystal fiber for coherent Raman endoscope[J]. Optics Express, 2011, 19(13): 12562-12568.
[167] Pshenay-Severin E, Bae H, Reichwald K, et al. Multimodal nonlinear endomicroscopic imaging probe using a double-core double-clad fiber and focus-combining micro-optical concept[J]. Light: Science & Applications, 2021, 10: 207.
[168] Ducourthial G, Leclerc P, Mansuryan T, et al. Development of a real-time flexible multiphoton microendoscope for label-free imaging in a live animal[J]. Scientific Reports, 2015, 5: 18303.
[169] Göbel W, Kerr J N D, Nimmerjahn A, et al. Miniaturized two-photon microscope based on a flexible coherent fiber bundle and a gradient-index lens objective[J]. Optics Letters, 2004, 29(21): 2521-2523.
[170] Lukic A, Dochow S, Bae H, et al. Endoscopic fiber probe for

nonlinear spectroscopic imaging[J]. Optica, 2017, 4(5): 496-501.
[171] Sung K B, Liang C, Descour M, et al. Near real time *in vivo* fibre optic confocal microscopy: sub-cellular structure resolved [J]. Journal of Microscopy, 2002, 207(2): 137-145.
[172] Sparks H, Kondo H, Hooper S, et al. Heterogeneity in tumor chromatin-doxorubicin binding revealed by *in vivo* fluorescence lifetime imaging confocal endomicroscopy[J]. Nature Communications, 2018, 9: 2662.
[173] Helmchen F, Fee M S, Tank D W, et al. A miniature head-mounted two-photon microscope: high-resolution brain imaging in freely moving animals[J]. Neuron, 2001, 31(6): 903-912.
[174] Myaing M T, MacDonald D J, Li X D. Fiber-optic scanning two-photon fluorescence endoscope[J]. Optics Letters, 2006, 31 (8): 1076-1078.
[175] Kim D, Kim K H, Yazdanfar S, et al. Optical biopsy in high-speed handheld miniaturized multifocal multiphoton microscopy [J]. Proceedings of SPIE, 2005, 5700: 14-22.
[176] Bird D, Gu M. Two-photon fluorescence endoscopy with a micro-optic scanning head[J]. Optics Letters, 2003, 28(17): 1552-1554.
[177] Herz P R, Chen Y, Aguirre A D, et al. Micromotor endoscope catheter for *in vivo*, ultrahigh-resolution optical coherence tomography[J]. Optics Letters, 2004, 29(19): 2261-2263.
[178] Fu L, Jain A, Xie H K, et al. Nonlinear optical endoscopy based on a double-clad photonic crystal fiber and a MEMS mirror [J]. Optics Express, 2006, 14(3): 1027-1032.
[179] Piyawattanametha W, Barretto R P J, Ko T H, et al. Fast-scanning two-photon fluorescence imaging based on a microelectromechanical systems two- dimensional scanning mirror[J]. Optics Letters, 2006, 31(13): 2018-2020.
[180] Zong W J, Wu R L, Li M L, et al. Fast high-resolution miniature two-photon microscopy for brain imaging in freely behaving mice[J]. Nature Methods, 2017, 14(7): 713-719.
[181] Fu L, Gu M. Fibre-optic nonlinear optical microscopy and endoscopy[J]. Journal of Microscopy, 2007, 226(3): 195-206.
[182] Jung J C, Mehta A D, Aksay E, et al. *In vivo* mammalian brain imaging using one- and two-photon fluorescence microendoscopy [J]. Journal of Neurophysiology, 2004, 92(5): 3121-3133.
[183] Murayama M, Larkum M E. *In vivo* dendritic calcium imaging with a fiberoptic periscope system[J]. Nature Protocols, 2009, 4 (10): 1551-1559.
[184] Cicchi R, Kapsokalyvas D, De Giorgi V, et al. Scoring of collagen organization in healthy and diseased human dermis by multiphoton microscopy[J]. Journal of Biophotonics, 2010, 3(1/2): 34-43.
[185] Adur J, Carvalho H F, Cesar C L, et al. Nonlinear optical microscopy signal processing strategies in cancer[J]. Cancer Informatics, 2014, 13: 67-76.
[186] Cicchi R, Massi D, Sestini S, et al. Multidimensional non-linear laser imaging of Basal Cell Carcinoma[J]. Optics Express, 2007, 15(16): 10135-10148.
[187] Lin S J, Jee S H, Kuo C J, et al. Discrimination of basal cell carcinoma from normal dermal stroma by quantitative multiphoton imaging[J]. Optics Letters, 2006, 31(18): 2756-2758.
[188] Provenzano P P, Inman D R, Eliceiri K W, et al. Collagen density promotes mammary tumor initiation and progression[J]. BMC Medicine, 2008, 6(1): 1-15.
[189] Matteini P, Ratto F, Rossi F, et al. Photothermally-induced disordered patterns of corneal collagen revealed by SHG imaging [J]. Optics Express, 2009, 17(6): 4868-4878.
[190] Sivaguru M, Durgam S, Ambekar R, et al. Quantitative analysis of collagen fiber organization in injured tendons using Fourier transform-second harmonic generation imaging[J]. Optics Express, 2010, 18(24): 24983-24993.
[191] Walker R F, Jackway P T, Longstaff D. Genetic algorithm optimization of adaptive multi-scale GLCM features[J]. International Journal of Pattern Recognition and Artificial Intelligence, 2003, 17(1): 17-39.
[192] Watson J M, Rice P F, Marion S L, et al. Analysis of second-harmonic-generation microscopy in a mouse model of ovarian carcinoma[J]. Journal of Biomedical Optics, 2012, 17(7): 076002.
[193] Zhuo S M, Chen J X, Wu G Z, et al. Quantitatively linking collagen alteration and epithelial tumor progression by second harmonic generation microscopy[J]. Applied Physics Letters, 2010, 96(21): 213704.
[194] Miljković M, Chernenko T, Romeo M J, et al. Label-free imaging of human cells: algorithms for image reconstruction of Raman hyperspectral datasets[J]. Analyst, 2010, 135(8): 2002-2013.
[195] Ozeki Y, Umemura W, Otsuka Y, et al. High-speed molecular spectral imaging of tissue with stimulated Raman scattering[J]. Nature Photonics, 2012, 6(12): 845-851.
[196] Zhang D L, Wang P, Slipchenko M N, et al. Quantitative vibrational imaging by hyperspectral stimulated Raman scattering microscopy and multivariate curve resolution analysis [J]. Analytical Chemistry, 2013, 85(1): 98-106.
[197] Ranjit S, Malacrida L, Jameson D M, et al. Fit-free analysis of fluorescence lifetime imaging data using the phasor approach[J]. Nature Protocols, 2018, 13(9): 1979-2004.
[198] Clayton A H A, Hanley Q S, Verveer P J. Graphical representation and multicomponent analysis of single-frequency fluorescence lifetime imaging microscopy data[J]. Journal of Microscopy, 2004, 213(1): 1-5.
[199] Monteleone A, Schary W, Wenzel F, et al. Label-free identification and differentiation of different microplastics using phasor analysis of fluorescence lifetime imaging microscopy (FLIM)-generated data[J]. Chemico-Biological Interactions, 2021, 342: 109466.
[200] Zhang Y D, Hato T, Dagher P C, et al. Automatic segmentation of intravital fluorescence microscopy images by K-means clustering of FLIM phasors[J]. Optics Letters, 2019, 44 (16): 3928-3931.
[201] Digman M A, Caiolfa V R, Zamai M, et al. The phasor approach to fluorescence lifetime imaging analysis[J]. Biophysical Journal, 2008, 94(2): L14-L16.
[202] Lee S H, Hong S H, Park S H, et al. Observation of cell division in a fertilized egg of a zebrafish by using a multimodal nonlinear optical microscope[J]. Journal of the Korean Physical Society, 2019, 75(6): 485-489.
[203] Xu X Q, Wang G X, Peng D Q, et al. Differentiation of early gastric cancer infiltration depths using nonlinear optical microscopy[J]. Journal of Physics D: Applied Physics, 2021, 54 (39): 394001.
[204] Zhang L L, Zou X, Huang J, et al. Label-free histology and evaluation of human pancreatic cancer with coherent nonlinear optical microscopy[J]. Analytical Chemistry, 2021, 93(46): 15550-15558.
[205] Li L H, Chen Z F, Wang X F, et al. Monitoring neoadjuvant therapy responses in rectal cancer using multimodal nonlinear optical microscopy[J]. Oncotarget, 2017, 8(63): 107323-107333.
[206] Teh S K, Zheng W, Li S X, et al. Multimodal nonlinear optical microscopy improves the accuracy of early diagnosis of squamous intraepithelial neoplasia[J]. Journal of Biomedical Optics, 2013, 18(3): 036001.
[207] Pallen S, Shetty Y, Das S, et al. Advances in nonlinear optical microscopy techniques for *in vivo* and *in vitro* neuroimaging[J]. Biophysical Reviews, 2021, 13(6): 1199-1217.
[208] Zhuo G Y, Spandana K U, Sindhoora K M, et al. Label-free multimodal nonlinear optical microscopy for biomedical applications[J]. Journal of Applied Physics, 2021, 129(21): 214901.
[209] Jose R J, Hyuk L J, Aneesh A, et al. Non-invasive monitoring

of pharmacodynamics during the skin wound healing process using multimodal optical microscopy[J]. BMJ Open Diabetes Research & Care, 2020, 8(1): e000974.
[210] Hou J, Williams J N, Botvinick E, et al. Visualization of breast cancer metabolism using multimodal nonlinear optical microscopy of cellular lipids and redox state[J]. Cancer Research, 2018, 78(10): 2503-2512.
[211] Yang L X, Park J, Marjanovic M, et al. Intraoperative label-free multimodal nonlinear optical imaging for point-of-procedure cancer diagnostics[J]. IEEE Journal of Selected Topics in Quantum Electronics, 2021, 27(4): 6801412.
[212] Zhang Y D, Guldner I H, Nichols E L, et al. Instant FLIM enables 4D *in vivo* lifetime imaging of intact and injured zebrafish and mouse brains[J]. Optica, 2021, 8(6): 885-897.
[213] Raspe M, Kedziora K M, van den Broek B, et al. siFLIM: single-image frequency-domain FLIM provides fast and photon-efficient lifetime data[J]. Nature Methods, 2016, 13(6): 501-504.
[214] He R Y, Xu Y K, Zhang L L, et al. Dual-phase stimulated Raman scattering microscopy for real-time two-color imaging[J]. Optica, 2016, 4(1): 44-47.
[215] Kong L J, Ji M B, Holtom G R, et al. Multicolor stimulated Raman scattering microscopy with a rapidly tunable optical parametric oscillator[J]. Optics Letters, 2013, 38(2): 145-147.
[216] Zhao Z W, Shen B L, Li Y P, et al. Deep learning-based high-speed, large-field, and high-resolution multiphoton imaging[J]. Biomedical Optics Express, 2023, 14(1): 65-80.
[217] Casacio C A, Madsen L S, Terrasson A, et al. Quantum-enhanced nonlinear microscopy[J]. Nature, 2021, 594(7862): 201-206.
[218] Qiu L D, Kang D Y, Wang C, et al. Intratumor graph neural network recovers hidden prognostic value of multi-biomarker spatial heterogeneity[J]. Nature Communications, 2022, 13: 4250.
[219] Hollon T C, Pandian B, Adapa A R, et al. Near real-time intraoperative brain tumor diagnosis using stimulated Raman histology and deep neural networks[J]. Nature Medicine, 2020, 26(1): 52-58.
[220] Huttunen M J, Hristu R, Dumitru A, et al. Multiphoton microscopy of the dermoepidermal junction and automated identification of dysplastic tissues with deep learning[J]. Biomedical Optics Express, 2019, 11(1): 186-199.
[221] Wang G X, Sun Y, Chen Y T, et al. Rapid identification of human ovarian cancer in second harmonic generation images using radiomics feature analyses and tree-based pipeline optimization tool[J]. Journal of Biophotonics, 2020, 13(9): e202000050.
[222] Zhang L L, Wu Y Z, Zheng B, et al. Rapid histology of laryngeal squamous cell carcinoma with deep-learning based stimulated Raman scattering microscopy[J]. Theranostics, 2019, 9(9): 2541-2554.
[223] 李浩宇, 曲丽颖, 华子杰, 等. 基于深度学习的荧光显微成像技术及应用[J]. 激光与光电子学进展, 2021, 58(18): 1811007.
Li H Y, Qu L Y, Hua Z J, et al. Deep learning based fluorescence microscopy imaging technologies and applications [J]. Laser & Optoelectronics Progress, 2021, 58(18): 1811007.

Review on Multimodal Nonlinear Optical Microscopy Imaging Technology

Li Yanping, Chen Yongqiang, Liu Yuqing, Hu Rui, Qu Junle, Liu Liwei*

College of Physics and Optoelectronic Engineering, Key Laboratory of Optoelectronic Devices and Systems of Guangdong Province and Ministry of Education, Shenzhen University, Shenzhen 518060, *Guangdong, China*

Abstract

Significance Nonlinear optical microscopy (NLOM) is a technology that combines nonlinear optical effect with optical microscopy to generate contrast images by nonlinear light-matter interactions. Additionally, NLOM differs from conventional microscopy, which is typically based on linear interactions such as absorption, scattering, refraction, and fluorescence. In the past few decades, nonlinear optical imaging techniques have become important tools for detecting biomolecules, cells, and tissues at the micrometer and nanometer levels. The NLOM advancements promote and enhance the basic research on biology, pharmacy, and medicine. The nonlinear imaging techniques mainly include second harmonic generation (SHG), third harmonic generation (THG), two-photon excited fluorescence (TPEF), three-photon excited fluorescence (3PEF), coherent anti-Stokes Raman scattering (CARS) microscopy, and stimulated Raman scattering (SRS) microscopy. These techniques rely on tight focusing of ultrashort pulses with high photon density to excite nonlinear processes, which feature diffraction-limited spatial resolution and optical sectioning. Additionally, nonlinear optical microscopes employ near-infrared light sources that provide strong penetration power and cause minimal photodamage to tissues, allowing label-free imaging at the subcellular level. The nonlinear optical properties of different molecules in biological tissues enable molecular specificity and selectivity, making nonlinear optical imaging techniques widely applicable in biomedical imaging.

With the advances in biology, the applications of nonlinear optical imaging technology are expanding, and the complex structures and functions of living organisms pose new challenges to optical imaging. Biomedical research requires super-composite optical imaging technology to achieve multidimensional optical characterization of biological tissues and obtain comprehensive information about their microstructure and molecular metabolism. Multiple nonlinear contrastive imaging technologies eliminate the need for tedious tissue preparation and enable analysis of unlabeled tissue samples,

which provides rich structural and functional information about complex organisms. Finally, the multimodal nonlinear optical imaging technology which integrates multiple optical characterization methods has emerged as a new direction in optical microscopy in recent years.

It is necessary to summarize and explore the existing research progress and future development trends to further promote the development of multimodal nonlinear optical imaging technology and contribute to relevant biomedical research. This will provide references for researchers in related fields.

Progress The generation of nonlinear optical effects relies on focusing ultrashort pulse lasers to achieve extremely high peak intensity. When multiple photons simultaneously interact with excited fluorophores or specific structures, nonlinear optical signals are generated by light-matter interactions. A deep understanding about the generation process of various nonlinear effects is necessary to obtain optical images with high signal contrast and signal-to-noise ratio (SNR). Furthermore, selecting appropriate excitation conditions and detection methods is crucial for effective nonlinear optical imaging. We introduce the generation process of different nonlinear optical signals and their imaging mechanisms, mainly including multiphoton excitation fluorescence (MPEF), SHG/THG, coherent Raman scattering (CRS), and two-photon fluorescence lifetime microscope (TP-FLIM).

Multimodal nonlinear optical imaging technology allows for accurate and comprehensive multi-parameter optical physical information. It serves as an important tool in studying complex organisms and multi-threaded dynamic processes from a multi-dimensional perspective. This technology has extensive applications in biological research fields such as physiology, neurobiology, embryology, and tissue engineering. However, different nonlinear optical imaging systems have distinct requirements for optics and hardware in excitation conditions and detection methods. Therefore, the key to integrating multiple nonlinear optical imaging technologies lies in coordinating the synchronous excitation of multiple nonlinear effects and the simultaneous detection of multi-dimensional signals. Meanwhile, we elaborate on the technical challenges and solutions related to multimodal coupling in nonlinear optical imaging and introduce the research progress and biological applications of multimodal imaging with multiple coupling mechanisms.

Additionally, we review the optimization schemes for multimodal nonlinear optical imaging from three aspects of imaging speed, spatial resolution, and SNR to further improve the performance of multimodal optical imaging system. System miniaturization is discussed, and multimodal nonlinear optical endoscopy is extended to enable dynamic monitoring of the epidermis and internal organs of living organisms. Furthermore, nonlinear optical imaging microscopes can visualize the tissue structure and molecules in organism specificity. The imaging results require combined image processing methods for the quantitative detection of biological molecules and tissue structures. Therefore, we further introduce quantitative analysis methods for different nonlinear optical images.

Conclusions and Prospects Multimodal nonlinear optical microscopy, along with corresponding quantitative analysis methods, can conduct imaging and characterize the structure and physiological dynamic processes of biological tissues from multiple information dimensions. It represents an important branch of nonlinear optical microscopy development, with extensive applications in biomedical fields such as cell detection, cancer diagnosis, and brain imaging. Additionally, it holds significant potential, particularly in clinical pathological diagnosis. However, there are still several aspects of this technology to be further developed and improved. Firstly, in multimodal imaging, TP-FLIM imaging based on time-correlated single photon counting (TCSPC) requires a longer accumulation time for photons to obtain the lifetime decay curve. Simultaneously, spectral scanning in stimulated Raman scattering (SRS) imaging necessitates changing the position of time delay displacement tables. The two imaging methods still limit the imaging speed of the system and hinder the multi-parameter optical characterization for certain dynamic physiological processes. Therefore, there is still a room for further research on fast multimodal nonlinear optical imaging schemes.

Meanwhile, in practical applications, the images obtained from multi-parameter nonlinear optical imaging systems should be combined with corresponding analysis methods to extract relevant biochemical information. This requires extensive data processing and statistical analysis, particularly in the context of clinical pathological analysis. Exploring new analytical methods that enable rapid conversion from optical images to biological information will significantly enhance the clinical applicability of multimodal nonlinear optical imaging. In summary, despite the potential and utility in biomedical research presented by multimodal nonlinear optical microscopy, further advancements are needed to address challenges such as imaging speed and data analysis. By developing faster imaging schemes and exploring new analytical methods, the clinical applications of multimodal nonlinear optical imaging can be greatly enhanced.

Key words imaging systems; microscopic imaging; nonlinear optics; multimodal optical imaging; optical endoscope